INDIANA UNIVERSITY

Development of Two Tools to Measure and Correct Betatron Tunes and Measure Transverse Emittances in the Fermilab Antiproton Accumulator

A DISSERTATION

SUBMITTED TO THE GRADUATE SCHOOL

IN PARTIAL FULFILLMENT OF THE REQUIREMENTS

for the degree

Masters of Science

Field of Physics

By

Allan Sondgeroth

Bloomington Indiana

May 2004

Contents

Acknowledgements

ABSTRACT

Development of Two Tools to Measure and Correct Betatron Tunes and Measure
Transverse Emittances in the Fermilab Antiproton Accumulator

Allan Sondgeroth

Tunes and emittances are both important beam parameters that must be known
and controlled in a circular particle accelerator, especially a storage ring such as
the Fermilab Accumulator. This thesis presents the development of two tools used
to measure and correct the tunes across the Fermilab Accumulator momentum
aperture. One of the tools also measures the emittances across momentum aperture.

CHAPTER 1

Introduction

1.1. Why Make an Antiproton Source?

The Fermilab Tevatron began operation as an 800 GeV fixed target machine, but the eventual goal was to use it as a proton-antiproton collider. Building on the CERN innovations and experiences, Fermilab began construction of an antiproton source. The first colliding beams in the Tevatron were established late in 1985 during a study period following a fixed target run. The antiproton source was commissioned and the first collider run began late in 1986. With a center of mass energy of 1.8 TeV (900 GeV on 900 GeV),the world's highest energy accelerator was again found at Fermilab. During Tevatron Run I, from 1992 through 1996, physics data was collected by to detector facilities, CDF and D0. Tevatron Run II began in 2001 and continues to date.

Luminosity is a measure of the number of collisions at an experiment. It is a function of beam intensity and beam emittance, which is related to the size of the beam. Through a series of improvements to Fermilab's accelerators, there has been steady improvement in the Tevatron's luminosity. During the 1988-89

Collider run, the design luminosity of $1.0\text{x}10^{30}\text{cm}^{-2}\text{sec}^{-1}$ was achieved. Since that time the luminosity has increased by more than a factor of 60. With the addition of the Main Injector and other accelerator improvements, the luminosity is expected to increase by another factor of 2. The addition of the Recycler ring should bring further improvements, perhaps as much as another factor of 2.

The FNAL Antiproton Source[1] is comprised of a series of beamlines leading from an upstream accelerator known as the Main Injector (MI) through a series of beamlines(P1, P2 and AP-1), the target station (Section 1.2), a beamline connecting the target station to the Debuncher ring(AP-2), the Debuncher ring (Section 1.3), a beamline connecting the Debuncher and the Accumulator ring(DtoA), the Accumulator ring (Section 1.4) and a beamline connecting the Accumulator to AP-1(AP-3). In a process called stacking (Section 1.5.1) antiprotons are created, accumulated, and stored in the Accumulator.

The largest bottleneck in a proton-antiproton collider is the time required to accumulate the required number of antiprotons. The process is inherently inefficient, typically for every 10^5 protons striking a target, only 1 or 2 antiprotons are captured and stored. It takes hours to build up a suitable stack to use for a colliding beams store. The performance of the antiproton source greatly affects the quality and duration of stores in the Tevatron. A loss of stored antiprotons or a beam with large emittances would contribute to a low integrated luminosity.

An undesirable tune value could lead to large emittances and beam loss. This paper outlines methods for measuring and measurements of the tunes for all beam energies in the Accumulator. Chapter 2 presents a method for calculating the tunes by measuring sideband frequencies at various revolution frequencies. The beam is moved using radio frequency (RF) cavities. Chapter 3 presents a method for calculating tunes and emittances by measuring integrated sideband power. Chapter 4 presents the lattice model and correction algorithms used to vary tunes and emittances.

1.2. Target station

The actual production and collection of antiprotons occur in a specially designed vault. The major components as seen by the incoming beam are:

- A stack of nickel disks, separated by copper cooling disks with channels for air flow to provide heat transfer. Standard sized target disks are about 10 cm in diameter and 2 cm thick. All disks have a hole in the middle to direct the air flow out of the assembly. The disks are held in a fixture that is encased in a thin titanium jacket. Motion control allows targeting of a specific disk.

- Immediately downstream of the target module is the Collection lens module. The lens is designed to collect a portion of the secondary particles coming

off of the target and render them parallel to each other. Electric current passing through the cylindrical lithium conductor produces a solenoidal magnetic field that focuses the negative secondaries. The lithium conductor is 15 cm long and 2 cm in diameter. The lens body is cooled with a closed loop cooling system. A pair of eccentric shafts is used to optimize the horizontal position and angle of the Collection lens.

- A 3-degree pulsed dipole follows the lens. Its purpose is to select 8 GeV negatively-charged particles and bend them into the AP2 line.

- A graphite-core beam dump which absorbs most of the particles not selected by the pulsed magnet. The dump is contained within several feet of steel shielding. A channel through the steel shield provides an exit for the 8 GeV negative beam and allows it to pass into the AP-2 line.

1.3. Debuncher

The purpose of the Debuncher is to accept pulses of antiprotons from AP-2 and reduce their momentum spread through RF bunch rotation and adiabatic debunching. This reduction of momentum spread is done to improve the Debuncher to Accumulator transfer because of the limited momentum aperture of the Accumulator at injection. The Debuncher also makes use of the time between Main Injector cycles to further reduce the momentum spread of the beam and to reduce the

transverse size of the beam through stochastic cooling[**2**]. This cooling greatly improves the efficiency of the Debuncher to Accumulator transfer.

1.4. Accumulator

1.4.1. Function

The purpose of the Accumulator is to accumulate antiprotons. This accumulation is accomplished by momentum stacking successive pulses of antiprotons from the Debuncher over several hours or days. Both radio frequency (RF) and stochastic cooling systems are used in the momentum stacking process. The RF decelerates the recently injected pulses of antiprotons from the injection energy to the edge of the stack tail. The stack tail momentum cooling system sweeps the beam deposited by the RF away from the edge of the tail and decelerates it towards the dense portion of the stack, known as the core. Additional cooling systems keep the pbars in the core at the desired momentum and minimize the transverse beam size.

What follows is a chronological sequence of events that takes place in the Accumulator:

(1) Unbunched antiprotons are extracted from the Debuncher, transferred down the Debuncher to Accumulator (DtoA) line, and injected into the Accumulator with a kinetic energy 8 GeV. The beam is transferred in the horizontal plane by means of a kicker and pulsed magnetic septum

combination in each machine (in order: D:EKIK, D:ESEPV, A:ISEP2V, A:ISEP1V and A:IKIK). Extraction in the Debuncher occurs just before another antiproton pulse arrives from the target.

(2) The Accumulator injection kicker puts the injected antiproton pulse onto the injection closed orbit which is roughly 80mm to the outside of the central orbit. The kicker is located in a high dispersion region so the higher energy injected beam is displaced to the outside of the Accumulator. This kicker is unique in that there is a shutter which moves into the aperture between the injection orbit and the circulating stacktail and stack. The shutter is in this position only when the kicker fires. The shutter's purpose is to shield the circulating antiprotons already in the Accumulator from fringe fields created when the kicker fires. Figure 1.1 diagrams a spectrum analyzer display of the Accumulator longitudinal beam distribution. It shows the relative location of the shutters in revolution frequency (which relates to the horizontal position in a dispersive region)

(3) After the injected pbars have been kicked onto the injection closed orbit, the shutter is opened and a 53 MHz RF system known as ARF-1 captures the beam in 84 bunches. ARF-1 then decelerates the beam by approximately 60 MeV to the edge of the stack tail, beyond the space occupied by the kicker shutter. The RF is adiabatically turned off as the edge of the tail
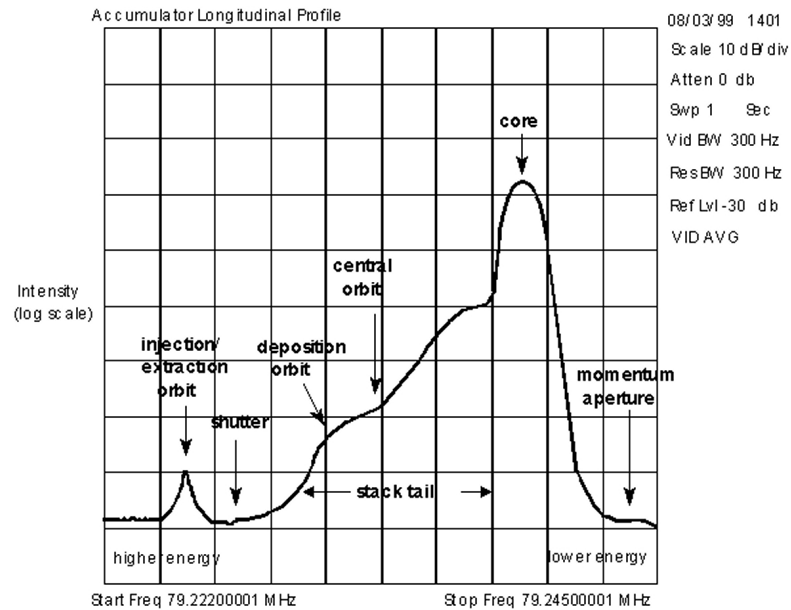
Figure 1.1. Spectrum Analyzer trace of a signal from a longitudinal Schottky detector showing the Accumulator momentum aperture during atiproton stacking.

is approached and the now unbunched pbars are deposited into the stack tail.

(4) The stack tail momentum cooling system now acts on the pbars. This system decelerates the beam towards the stack core which is approximately -150 MeV from the injection orbit (or ˜63 mm to the inside of the Accumulator central orbit in a high dispersion region).

(5) After approximately 30 minutes, the antiprotons in the stack tail have been decelerated into the domain of the core cooling systems. Six stochastic

cooling systems act on beam in the core during stacking. The 4-8 GHz core momentum systems control the momentum spread and keeps the pbars from hitting the low momentum aperture. The 4-8 GHz, in 3 bands, core horizontal and vertical betatron cooling systems keep the transverse emittances minimized.

(6) This process continues for hours or days with the stack growing in size until the desired Accumulator intensity is reached or the Tevatron needs to be refilled.

(7) When a transfer of pbars to the Main Injector is desired, an RF system known as ARF-4 is utilized. ARF-4 has a harmonic number of h=4 and is energized at a very low amplitude at a frequency corresponding to that of the revolution frequency of beam in the core. The RF voltage is slowly increased and a portion of the beam in the core is captured into four buckets and is slowly moved through the stack beyond the space occupied by the shutter, and onto the extraction orbit (at the same frequency as the injection orbit).

(8) Once the unstacked bunch is on the extraction orbit, the ARF-4 voltage is increased. The additional voltage acts to shrink each bunch longitudinally, giving them the same distribution in time as 10-12 Main Injector 53 MHz bunches.

(9) Like its injection counterpart, the extraction kicker has a shutter to shield the remaining stack from fringe fields. The extraction kicker shutter closes, then the kicker is fired. The deflection imparted by the kicker provides sufficient horizontal displacement to place the kicked beam in the field region of a Lambertson magnet which bends the beam up out of the Accumulator and into the AP3 line.

1.4.2. Lattice

The Accumulator "ring" actually resembles a triangle with flattened corners. The lattice has been designed with the following constraints in mind:

- The Accumulator must be capable of storing an antiproton beam over many hours.

- There must be several long straight sections of lengths up to 16 m with small transverse beam sizes to accommodate stochastic cooling pickups and kickers.

- Some of these sections must have low dispersion, others with dispersion of about 9 m (high dispersion).

- Betatron cooling pick-ups and kickers must be an odd multiple of $\pi/2$ apart in betatron phase (i.e. the number of betatron oscillations) and far enough apart physically so that a chord drawn across the ring will be

significantly shorter than the arc. Cooling pickup signals must arrive at the kickers on the same turn in time to act on the particles that created the signal.

The end result is that the Accumulator has an unconventional triangular shape that includes 6 straight sections with alternately low and high dispersion.

The dispersion function (often written η_x or η_y) describes the contribution to the transverse size of a particle beam as a result of its momentum spread. Dispersion is caused in large part by bending magnets, as different momenta particles are bent at different angles as a function of the momentum. In a low dispersion area, the beam size is almost entirely defined by the β function and the normalized emittance of the beam. In a high dispersion region, the beam size is defined by the β function and normalized emittance as well as the dispersion function. In the case of the Accumulator, the horizontal β function is small in the high dispersion regions in addition to the large horizontal dispersion function so the beam size is dominated by $\frac{\Delta p}{p}$ and the position errors are dominated by off momentum particles. As a result, the beam size is very small in the low dispersion areas and very wide horizontally in the high dispersion areas (there is very little vertical dispersion due to the fact that there are only small vertical trim dipoles in the Accumulator).

10

A10

A1Q1 (QF)

A1Q2 (QD)

Sextupole →

A1Q3 (QF)

A1B3 (Dipole)

A1Q4 (QF)

A1Q5 (QD)

A1Q6 (QF)

Sextupole →

A1Q7 (QD)

A1B7 (Dipole)

A1Q8 (QF)

A1B8 (Dipole)

A1Q9 (QD)

Sextupole →

A1B9 (Dipole)

A1Q10 (QF)

A1B10 (Dipole)

Sextupole/
Octupole

A1Q11 (QF)

A1Q12 (QD)

A1Q13 (QD)

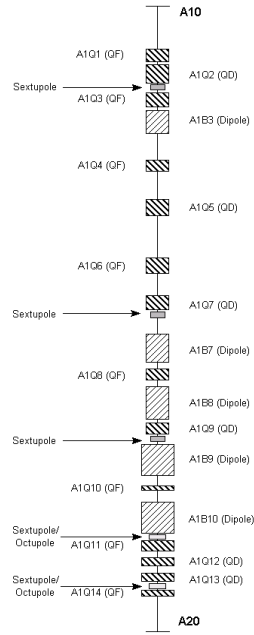Sextupole/
Octupole

A1Q14 (QF)

A20

Figure 1.2. Accumulator lattice for the A10 sector. This represents one-sixth of the ring. The A20 sector is mirror symmetric.

Low dispersion regions can be used by cooling systems to sense a beam position error due to transverse oscillations. In the case of the Accumulator, betatron cooling system pickups are best placed in low dispersion straights while momentum cooling pickups are found in one of the high dispersion straight sections.

There are special arrangements of quadrupoles approaching the straight sections in order to achieve the desired dispersion. The Accumulator has mirror symmetry about the straight sections. The magnet numbering scheme increases as one travels in the pbar direction in the odd-numbered sectors, and decreases in the even
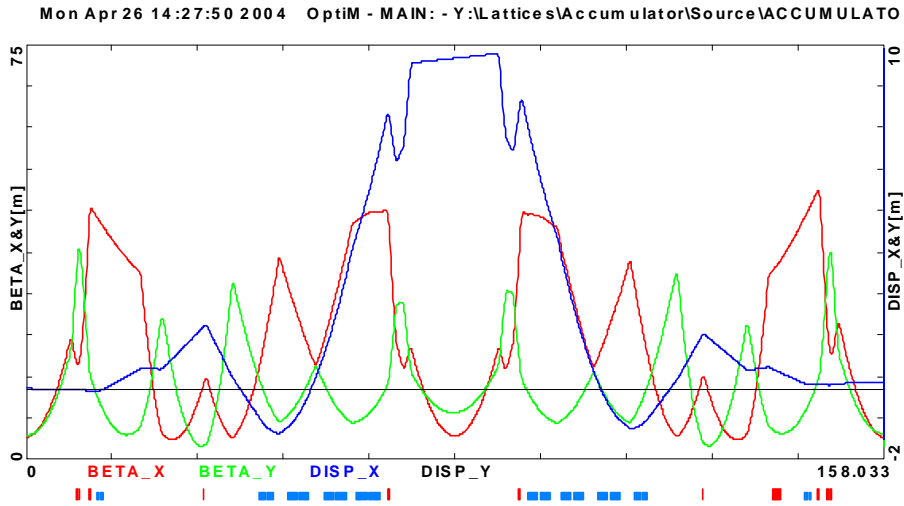
11

Figure 1.3. Plot of the beta and dispersion funtions for 2 sectors of the Accumulator. The red trace is β_x. The green trace is β_y and the blue trace is D_x.

sectors. The lattice of one sector (one-sixth) of the Accumulator is shown in Figure 1.2. The beta functions and dispersion for 2 sectors of the Accumualtor are shown in Figure 1.3 .

The Accumulator straight sections are full of specialized devices. A10 contains core betatron cooling pickup tanks, Schottky and other diagnostic pickups, damper pickups and kickers as well as the beam current transformer for measuring the circulating beam intensity. The injection and extraction kickers are found in straight section A20 as are the pickup arrays for the 4-8 GHz core momentum cooling system. In A30 reside the extraction Lambertson magnetic septum, the stack tail momentum, 2-4 GHz core momentum, and core betatron cooling kickers.

Section A40 contains a beam scraper used for measuring $\Delta p/p$ and a set of flying wires for making high dispersion measurements of the beam size. A50 contains transverse scrapers. The various Accumulator RF cavities are also found in A50. Just upstream of the actual straight section is the kicker tank for the 4-8 GHz core momentum system and a set of flying wires for making low dispersion measurements of the beam size. Straight section A60 contains all of the stochastic cooling pickups for the stack tail momentum systems and the 2-4 GHz core momentum cooling.

The Accumulator is operated in two configurations, a stacking lattice and a shot lattice. The slip factor η(eta), the amount one particle slips past another in longitudinal phase space as particles travel around the ring, is changed between the two configurations by ramping the fields in the magnetic elements. For the stacking lattice η = -0.012 which optimizes the stacktail cooling and allows for the highest stacking rates. For the shot lattice η = -0.024 which lowers the emittances of the beam and produces better beam brightness for the Tevatron.

1.5. Modes of Operation

The Antiproton source can be oriented into several modes of operation based on the needs of users. In addition to antiproton stacking and unstacking, several operating modes were created that utilize protons. Protons provide a convenient

source of relatively high intensity beam for tune-up and studies. For the RF tune measurement method, the beam can be protons or antiprotons circulating in the Accumulator.

1.5.1. Antiproton Stacking

Protons are accelerated in the Main Injector to 120 GeV. After the protons are bunch rotated, the short bunch length beam is extracted from the Main Injector. Beam is transported, through a series of beamlines, into the AP-1 line (see Figure 1.4). The protons move down the AP-1 line into the target vault where the beam strikes a nickel target. Downstream of the target, 8 GeV antiprotons, as well as other negative secondaries, are focused with the collection lens and are momentum selected with a pulsed magnet. Particles that are off-momentum or positively charged are absorbed in a beam dump. The secondary beam travels to the Debuncher via the AP2 line where most of the secondaries, that are not antiprotons, decay away. Of the remaining secondaries, most are lost in the first dozen turns in the Debuncher. Only the small fraction of antiprotons with appropriate energy survive to circulate in the Debuncher. For every million protons on target, only ˜20 antiprotons circulate in the Debuncher. After debunching and cooling in the Debuncher, the antiprotons pass through the D to A line and into the Accumulator. Successive pulses of antiprotons arriving into the Accumulator
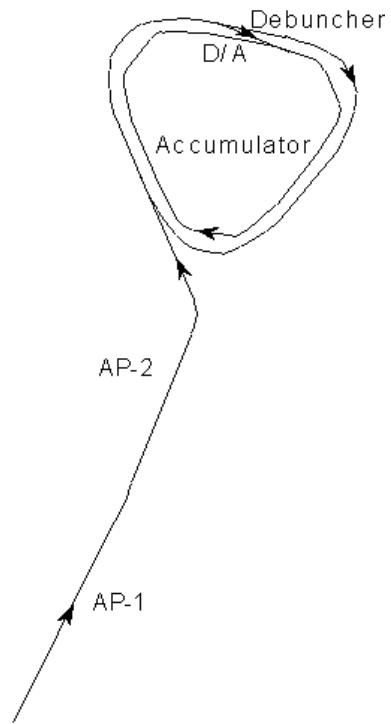
Figure 1.4. Path of antiprotons in stacking mode.

are 'stacked' over several hours or days into the core by ARF-1 and stochastic cooling. Stacking cycles are at least 1.5 seconds in duration and may be extended to improve the stacking rate with larger stacks.
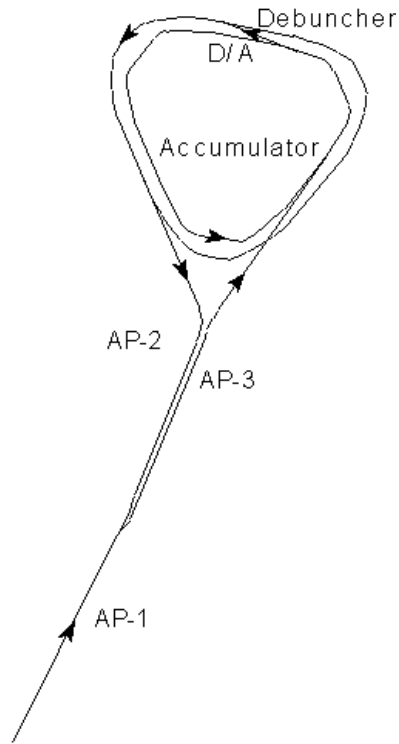
Figure 1.5. Path of protons in reverse proton mode.

1.5.2. Reverse Protons

8-GeV protons from the Main Injector are transported, through a series of beamlines, into the AP-1 line. Beam is bent into the AP-3 line bypassing the vault. After passing through AP-3 the beam continues through a C-magnet and the field region of the extraction Lambertson which bends the beam upward into the Accumulator at A30. The extraction kicker in A20 deflects the beam horizontally onto the closed orbit of the Accumulator(see Figure 1.5).
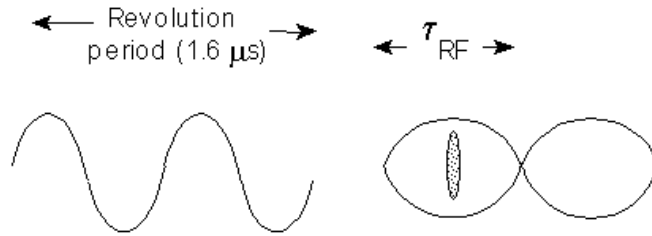
16

Figure 1.6. ARF-3 RF structure.

Reverse protons are used in Collider mode to tune up the AP-1 and AP-3 lines prior to an antiproton transfer from the Accumulator to the Main Injector. Reverse proton mode is also used for high intensity studies in both rings and all beamlines. If desired, particles can be extracted from the Accumulator and sent down the D to A line into the Debuncher. Beam can then be injected backwards into the AP-2 line and transported to the target vault.

1.6. Tools Used for Measurements

1.6.1. ARF-3

ARF-3 is a $h = 2$ ($1.26 MHz$) RF cavity (Figure 1.6) that is used to move the beam to various revolution frequencies in the Accumulator for measurements and studies.

The low level amplitude input to ARF-3 comes from either a digital to analog converter (DAC) or a programmable ramp card. The frequency inputs are provided by a digital synthesizer.

1.6.2. Vector Signal Analyzer

Signals from the Schottky detectors (Section 1.6.5) can be displayed on a Hewlett Packard HP 89440A DC-1800 MHz Vector Signal Analyzer (VSA). A coaxial relay multiplexer is used to connect the Schottky detector to the VSA. The HP 89440A is capable of measuring rapidly time-varying signals and addresses problems dealing with complex modulated signals that cannot be defined in terms of simple AM, FM, or RF. It uses a large parallel digital filter array at its input and performs a Fast Fourier Transform (FFT) to display an amplitude versus frequency spectrum[3].

1.6.3. ACNET

The accelerator controls network (ACNET) is a general term used to describe the overall controls system. There is a VAX cluster provided for code development of console applications and for using several of the control system public facilities. This cluster is called ADCON.

1.6.3.1. Architecture. The control system consists of four main components: front-ends, centrals, consoles and the network that ties them all together. Front-ends are the computers that bridge between the hardware (e.g. power supply control cards, analog read-backs, etc.) and the rest of the control system. Centrals are the machines that provide centralized, shared tasks such as databases, shared files, alarm reporting, etc. Consoles are the computers that an end-user (e.g. an Accelerator Operator) uses to control the accelerator. They provide a user interface to present accelerator data. Consoles communicate with the front-ends and the centrals to acquire and scale data. The network is the hardware and software that connect consoles, centrals and front-ends; allowing them a means to communicate with each other.

1.6.3.2. Consoles. A console is the machine and system software that provide the human interface to the accelerator. There are a fixed number of processes that define a console including several system tasks and a fixed number of application programs.

There are two main kinds of applications that run on a console: Primary Application (PA) and Secondary Application (SA). PAs run with character-based windows and take keyboard input. SAs runs with graphics based windows and usually do not use keyboard input. There are 3 PAs and 3 SAs allowed to run on

a given console. SAs are started from an existing PA. PAs also have the ability to use two dedicated screens which are pixel based, for graphics and text display.

1.6.3.3. Devices. Devices are an important logical construct within the control system. A device is the common way to address a physical channel (hardware). More specifically, 'device' refers to an ACNET device in the database. A device is identified by a unique integer (called a device index, or DI) or a name. Devices are defined to have some set of properties (PIs): reading, setting, basic status, basic control, analog alarm, digital alarm, etc. By addressing a DI/PI combination one can read or set that part of a device. Device properties can also have scaling information stored in the database.

1.6.4. Programmer Tools

There are a large set of library routines provided for the console application programmer. This library is called CLIB (Console LIBrary). CLIB contains routines for user interface, data acquisition and program control.

1.6.5. Schottky Signals

A charged particle passing through a resonant stripline detector or a resonant cavity creates a short signal pulse. A particle beam is made up of many charged

particles. Each particle creates a short signal pulse. This collection of pulses is known as a Schottky signal (a more complete description is given in Section 3.1).

There are three Schottky detectors used in the Accumulator. The vertical, horizontal and longitudinal detectors are located in the A10 straight section. The vertical and horizontal transverse pickups are approximately 24 inches long and 2 inches in diameter. These pickups detect transverse beam oscillations. The vertical pickup has the striplines above and below the beam with outputs on the top and bottom, the horizontal pickup is rotated 90°. The transverse pickups are a stainless steel tube with a slot cut along much of the long dimension (see Figure 1.7). The pickup is held by ceramic rings, which also electrically insulate it from the outer housing.

Signals from each plate are fed through to a 3/8-inch heliax cable, which is run to the AP-10 service building. The detectors resonate at a frequency determined by the length of the strip inside the cylinder plus the coaxial cable between the output connector and a capacitor. Connectors in the middle are used to inject a signal for tuning the device to the frequency of interest. Horizontal and vertical pickups are mounted on motorized stands so that the device can be centered with respect to the beam.

The longitudinal pickups are larger, 37 inches in length and 3.4 inches in diameter. These pickups are tuned quarter-wave cavities that are made by separating
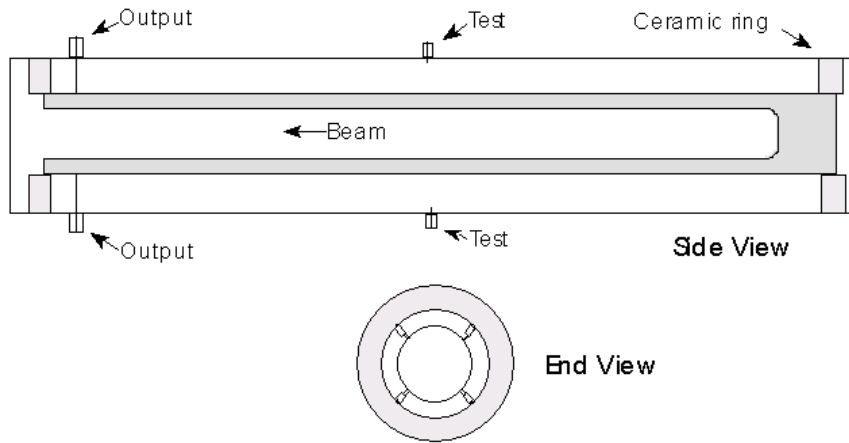
Figure 1.7. Diagram of a Schottky detector.

a stainless steel tube into two sections with a ceramic across the gap. Charged particles crossing the gap produce Schottky signals. The longitudinal detectors are tuned with plungers or sliding sleeves on the center element.

The Schottky detectors used in the Antiproton Source are tuned to the 126th harmonic of the beam's revolution frequency. There are several reasons for choosing the 126th harmonic for the design of the Schottky detectors. The spectral power contribution from the 53.1 MHz bunch structure (from ARF-1 in the Accumulator) is minimized by using a frequency located between 53.1 MHz (h=84) and its second harmonic at 106.2 MHz (h=168). The resulting signal from the revolution harmonic for the Accumulator core would be 126*.628881 MHz = 79.239 MHz. The physical size of the detector must also be taken into account. The aperture

must be large enough to not restrict beam transmission. Limited space available in the rings limits the pickup length to only 1 or 2 m. Schottky detectors designed for the 126th harmonic fit both of these size constraints. For example, recall that the longitudinal Schottky pickups are 1/4 wavelength long. The physical length of the cavity as built is 0.94 meters which would result in a resonant frequency of:

(1.1) $$f = \frac{velocity}{length} \sim \frac{3E8m/s}{4*.94m} \sim 79.75MHz$$

That works well for the Accumulator.

1.7. Accumulator Betatron Tunes

As particles travel around the ring they oscillate about the machine design trajectory. This motion is termed a betatron oscillation. The number of betatron oscillations per revolution is termed the betatron tune. There is a betatron tune for both the x and y planes. The integer number of betatron tunes are measured by changing the magnetic field of one dipole and counting the oscillations on a beam position monitor (BPM) display. The plots in Figure 1.8 show 6 full oscillations (Q_x) about the design and 8 full oscillations (Q_y) about the design orbit in the y plane.

Figure 1.8. Difference orbits showing oscillations about the machine design orbit caused by dipole deflections. The plot on the left shows a horizontal deflection. The plot on the right shows a vertical deflection.

The fractional parts of the peak tunes (q_x, q_y) on the core revolution frequency are calculated from Schottky dectector signals, as displayed in Figure 1.9 , using Equation 1.2. Here q_x is calculated to be 0.6969 and q_y is calculated to be 0.6845.

(1.2) $$q_x = \frac{P_x}{f_{rev}} \qquad q_y = \frac{P_y}{f_{rev}}$$

where P_x, P_y and f_{rev} are the horizontal sideband peak frequency, vertical sideband peak frequency and core revolution frequency respectively. Combining the integer tune measurements with the fractional tune measurements shows that $Q_x + q_x = 6.6969$ and $Q_y + q_y = 8.6845$.
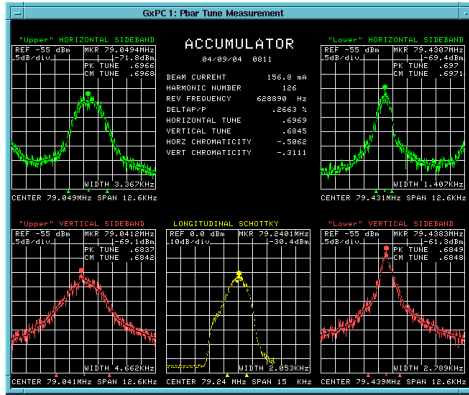
Figure 1.9. Spectrum analyzer display of a core revolution frequency fractional tune measurement.

Betatron orbit distortions occur as particles travel around the ring due to magnet construction and alignment errors. For particles with an integer tune these orbit distortions would reinforce on every turn around the ring until the distortions become large enough to cause the particles to strike the walls of the vacuum chamber. This condition is termed a resonance[**4**]. The integer tune is the most elementary, and strongest, example of a tune resonance. Other strong resonances would be tune values of one-half integer, one-third integer and one-fourth integer. Figure 1.10 shows the core horizontal and vertical fractional tunes with respect to the horizontal and vertical machine resonance tune lines, termed the tune space. The Accumulator operates between the two-thirds resonance and the five-sevenths resonance in tune space.
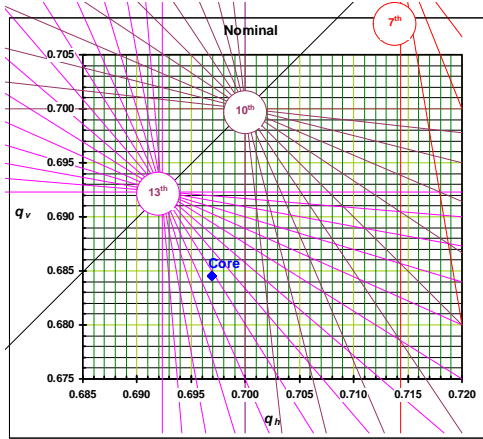
Figure 1.10. The horizontal and vertical fractional tune with respect to resonance lines. The x axis is the fractional horizontal tune. The y axis is the fractional vertical tune.

1.8. Transverse Emittances

In general a beam of particles can be characterized in detail by its density in the six-dimensional phase space[**5**], (x, p_x, y, p_y, z, p_z), where p is momentum. In practice the six-dimensional description is split into three two-dimensional subspaces, (x, p_x), (y, p_y), and (z, p_z), where x is the horizontal plane, y is the vertical plane and z is the longitudinal plane. The convenient notation (x, x') and (y, y') is used for the transverse vectors, where $p_x = mc\beta\gamma x'$ and $p_y = mc\beta\gamma y'$, β and γ are the Lorentz factors. The particles in the beam form an ellipse in each transverse phase space as shown in Figure 1.11. The emittance (ε) is defined in terms of the area occupied by the beam in these two-dimensional spaces. The 95% emittance value is used at Fermilab.
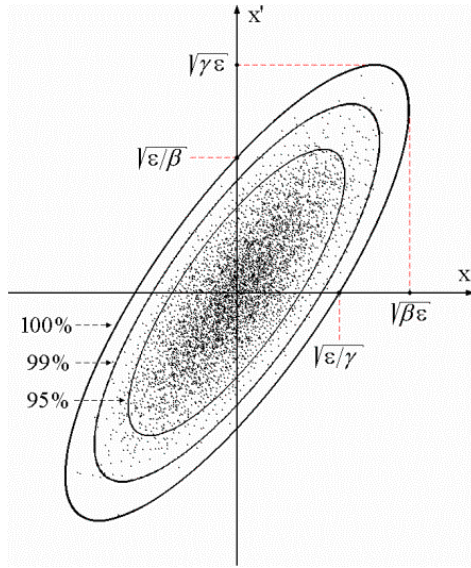
Figure 1.11. Horizontal phase space as it relates to the Lorentz factors.

Large transverse emittances in the stack could lead to beam loss, poor brightness and low luminosity in the Tevatron. The transvers emittances of the stack are monitored on a consistant basis by a dedicated system and are normalized to the number of antiprotons in the stack. Transverse emittance sizes range from $0 \ \pi \ mm \ mr$ with no stack to $1.7 \ \pi \ mm \ mr$ and $1.3 \ \pi \ mm \ mr$ for horizontal and vertical, respectively, with a stack size of $200m$ A.

CHAPTER 2

Tunes vs Revolution Frequency Moving Beam with ARF-3

The tunes vs revolution frequency moving beam with ARF-3 (RF method) is used when the Antiproton Source is not in stacking operations. Beam is expected to be circulating in the Accumulator. The beam is bunched, using ARF-3, and moved in steps through a frequency range in the momentum aperture. Schottky detectors are connected, one at a time, to a VSA. Trace data is stored and a contour plot is displayed showing the sideband tunes versus revolution frequency. Protons or antiprotons may be used. Antiprotons are used when the stack is small, such as just after a store has begun. Protons are used when the machine is configured in the reverse proton mode. One measurement, using both upper and lower sidebands, takes approximately 25 minutes. This includes bunching the beam, making the measurements, moving the beam back to the original revolution frequency and debunching the beam.

An ACNET program written in C was created to accomplish this task. Table 2.1 lists user controlled parameters.

Parameter	Choices	Default
Sidebands to scan	upper, lower or both	upper
Horizontal sideband harmonic	any positive integer	126
Vertical sideband harmonic	any positive integer	126
Number of VSA trace averages	any positive integer	25
VSA input sensitivity upper limit	-30 to 30 dbm	-15 dbm
Lower tune limit	any positive fraction	0.667 (2/3)
Upper tune limit	any positive fraction	0.714 (5/7)
Number of VSA frequency points	201, 401, 801, 1601	801
Percent of signal strength to plot	any positive value	90
Number of contours to plot	any positive value	20
Revolution frequency of beam (f_{rev})	628700-629000 Hz, auto	auto
First scan revolution frequency	628700-629000 Hz	628895 Hz
Last scan revolution frequency	628700-629000 Hz	628750 Hz
Bunching voltage	any, auto	auto

Table 2.1. Moving Beam with ARF-3 Method Parameter List

To ensure the beam is not lost or diffused once the user starts a measurement all cooling and RF systems are turned off and shutters are opened.

2.1. VSA Setup

The VSA is initialized and setup as follows;

- Set to vector mode

- GPIB data format set to 64 bit real

- Number of frequency points set

- Trace coordinates set to log-magnitude

- Upper limit of the analyzer input's sensitivities range set to –15 dBm

- Number of averages set

- Averaging turned on

If the current revolution frequency or the bunching volts are set to auto the following steps are taken;

- Center frequency set to 79.2288 MHz

- Span set to 26 KHz

2.2. Measuring the Beam Revolution Frequency and Width

If the current revolution frequency or the bunching voltage are set to auto, the longitudinal Schottky detector is connected to the VSA. This setup will allow the VSA to sense the entire momentum aperture. A delay is given to allow the VSA to average. The display is paused and the trace recorded. The program scans

through the trace data, point by point, to find the VSA frequency at the peak of the spectrum. The revolution frequency is calculated using Equation 2.1,

(2.1)
$$P_{Beam} = P_{VSA} \div 126$$

where P_{VSA} is the VSA frequency of the signal peak and P_{Beam} is the revolution frequency of the signal peak

The frequency width of the beam is needed to calculate the amount of voltage required to bunch the beam. The beam width is defined to be the frequency span of the points at or above a 10 dB power level above the noise floor of the signal. To calculate the noise floor the VSA measurements are restarted and the center frequency is set to 79.5432 MHz. This frequency is between the 126th and 127th harmonic where there is no beam signal. A delay is given to allow the VSA to average. The display is paused and the trace recorded. The noise floor is calculated using Equations 2.2.

(2.2)
$$N_F = N_{Ave} + (2 \times N_{RMS})$$

where

$$N_{Ave} = N_{Sum} \div (S_P - 1),$$

$$N_{RMS} = \sqrt{N_{Sum^2}} \div (S_P - 2)$$

and N_{Sum} is the sum of all VSA points, N_{Ave} is the noise average, M_{VSA} is the VSA point measurements minus N_{ave}, N_{Sum^2} is the sum of all $(M_{VSA})^2$, N_{RMS} is the rms noise, N_F is the noise floor and S_P is the number of VSA signal points.

Once the noise floor is calculated the frequencies in the array containing the beam are converted to revolution frequencies and the trace is searched. Since the Accumulator operates above transition the high energy, low frequency, side of the beam is found by comparing the power at each VSA point to the noise floor power starting from the peak moving down in frequency and including each point until the power is less than 10 dB above the noise floor. Likewise, the low energy, high frequency, side of the beam is found by comparing the power at each VSA point to the noise floor power starting from the peak moving up in frequency and including each point until power is less than 10 dB above the noise floor. The beam width is the difference between these two frequencies.

2.3. Calculating the Bunching Voltage

The bunching voltage is calculated using Equations 2.3.

(2.3)
$$V_{RF} = (\frac{1.2}{64}\omega_{RF}\frac{\varepsilon_L}{\beta_s})^2(2\pi h\frac{\eta}{e_c E_s})$$

where,

$$E_s = \sqrt{(pc)^2 + (m_p c^2)^2},$$

$$\gamma_s = \frac{E_s}{m_p c^2},$$

$$\beta_s = \sqrt{1 - \frac{1}{\gamma_s^2}},$$

$$\varepsilon_L = \frac{\beta_s^2 E_s}{\eta}(\frac{f_{rev}}{\Delta f_{rev}^2}),$$

$$\omega_{RF} = 2\pi h f_{rev}$$

and h is the RF harmonic, p is the orbit beam momentum, η is the lattice slip factor, f_{rev} is the beam revolution frequency, Δf_{rev} is the beam width, L is the

orbit length, m_p is the antiproton mass, c is the speed of light, E_s is the synchronous energy, γ_s is the relativistic gamma, β_s is the relativistic beta, ε_L is the longitudinal emittance, ω_{RF} is the angular RF frequncy and e_c is the electron charge.

2.4. Bunching the Beam

Depending on the initial setup the beam is adiabatically bunched, using the relationships in Equations 2.4 , at either the calculated or user selected revolution frequency.

(2.4)
$$V(t) = \frac{V_0}{(1 - \omega_s At)^2}$$

where

$$\omega_s = \sqrt{\eta f_{rev} \omega_{RF} e_c \frac{V_0}{\beta_s^2 E_s}}$$

and V_0 is the intitial voltage, A is the adiabatic constant, t is the time and $V(t)$ is the voltage at given time t.

2.5. Measuring the Sidebands

The beam is moved, using the ARF3 system, to the revolution frequency of the first scan point. The VSA is connected to the horizontal Schottky detector. As the tune of the beam increases the sidebands move further away from the revolution

frequency. The upper sideband will move higher in frequency while the lower sideband will move lower in frequency. If the upper sidebands have been selected the VSA start and stop frequencies are set to reflect the lower and upper tune values, respectively, at the first scan revolution frequency. They are calculated using Equations 2.5:

(2.5)
$$H_{Start} = ((H_h - 1) + \nu_{Lower})f_{rev},$$

$$H_{Stop} = ((H_h - 1) + \nu_{Upper})f_{rev},$$

$$V_{Start} = ((V_h - 1) + \nu_{Lower})f_{rev},$$

$$V_{Stop} = ((V_h - 1) + \nu_{Upper})f_{rev}$$

where H_h is the harmonic for the horizontal sideband, V_h is the harmonic for the vertical sideband, H_{Start} is the VSA horizontal start frequency, V_{Start} is the VSA vertical start frequency, H_{Stop} is the VSA horizontal stop frequency, V_{Stop} is the

VSA vertical stop frequency, ν_{Lower} is the lower tune limit and ν_{Upper} is the upper tune limit.

If the lower sidebands have been selected the VSA start and stop frequencies are set to reflect the upper and lower tune values, respectively, at the first scan revolution frequency. They are calculated using Equations 2.6:

(2.6)
$$H_{Start} = ((H_h + 1) - \nu_{Upper})f_{rev},$$

$$H_{Stop} = ((H_h + 1) - \nu_{Lower})f_{rev},$$

$$V_{Start} = ((V_h + 1) - \nu_{Upper})f_{rev},$$

$$V_{Stop} = ((V_h + 1) - \nu_{Lower})f_{rev}$$

A delay is given to allow the VSA to average. A trace is recorded and saved into an array. Each sideband has a unique array. If both sidebands are chosen, the upper sideband is measured first. The lower sideband is measured second. The VSA is then connected to the vertical schottky detector. Vertical sideband data

is recorded in the same fashion. The bunched beam is then moved in frequency to subsequent points. At each point the above process is repeated.

2.6. Plotting the Data

When the last scan point has been completed the noise floors for the selected sidebands are calculated using Equation 2.2 and the data arrays are searched to find the peak values. The difference between the peak and the noise floor gives the signal strength for each sideband. Contour values are calculated as shown in Equations 2.7. Colors are chosen as displayed by Table 2.2:

(2.7) $$C_d = S_\% \times S_s,$$

$$C_{dv} = C_d \div N_c,$$

$$C_v(1) = P,$$

$$C_v(n) = C_v(n-1) - C_{dv}$$

Contour Color	Contour Value (% of Peak Signal Strength)
White	86-100
Yellow	72-86
Red	58-72
Magenta	44-58
Green	30-44
Cyan	16-30
Blue	0-16

Table 2.2. Contour Colors

where S_s is the signal strength, C_d is the contour depth, $S_\%$ is the percent of signal strength to plot, N_c is the difference in contour levels, $C_v(n)$ is the number of contours to plot, $C_c(n)$ is the array of contour colors and P is the peak of the signal strength.

Separate PA graphics screens are opened for upper sidebands and lower sidebands. Each screen has a plot for horizontal tunes and vertical tunes. Each plot is setup to display tunes on the y-axis and revolution frequency on the x-axis. The results, using the default settings of 90% peak signal strength and 20 contours, are displayed in the plot windows as shown in Figure 2.1.The data was taken on 12/09/03. Before the measurement was taken there were 12 mA of antiprotons circulating on the core revolution frequency of 628887 Hz with the Accumulator configured on the stacking lattice. The measurement took ~25 minutes to complete.
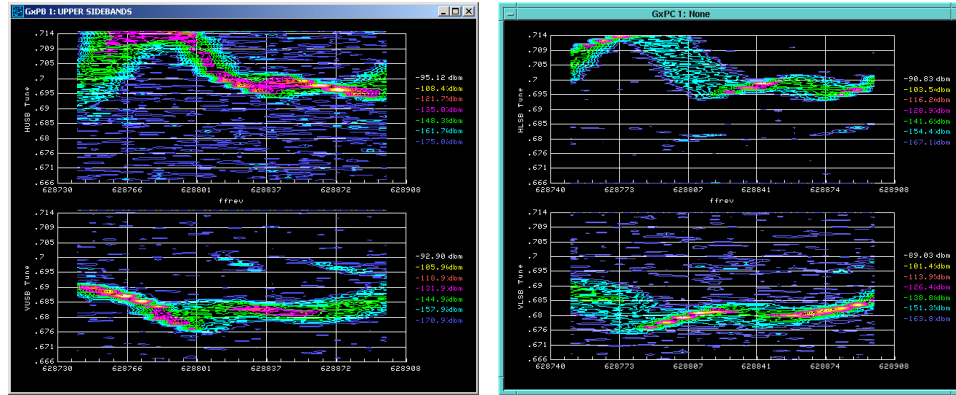
Figure 2.1. Horizontal and vertical sideband tunes. The vertical
axis shos the fractional tune value between the two-thirds and
five-sevenths resonances. The horizontal axis shows the Accumulator
revolution frequency. The injection frequency is 628765 Hz and the
core revolution frequency is 628888 Hz. 90% of the peak signal
strength and 20 contours are plotted. The plot on the left are the
upper sidebands. The plot on the right are the lower sidebands.

Coupling is evident near the core revolution frequency, especially in the vertical

tune measurement.

2.7. Options After the Initial Measurement

After the intial measurement is complete the user may choose to do any of the

following:

- Save the measurement for later analysis.

- Make another measurement moving the beam in the opposite direction.

- Replot the data using different signal depths and number of contours (

  Section 2.8).

39

- Move the beam back to the original revolution frequency and debunch.

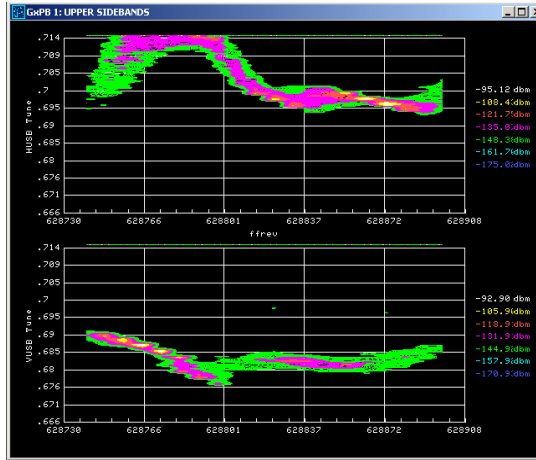- Use a model of the lattice to simulate changes in the tunes vs revolution frequency (Section 2.9).

Figure 2.2. Upper horizontal and vertical sideband tunes. 70% of the peak signal strength and 50 contours are plotted.

2.8. Replot the Data

By changing the depth of the signal and number of contours to plot the user can explore different aspects of the measurement. Figure 2.2 shows the upper sidebands with 70% of the peak signal depth and 50 contours plotted. While Figure 2.2 is a cleaner plot and more clearly shows the features near the peak signal values the plot for the vertical upper sideband in Figure 2.1 shows the evidence of coupling with the horizontal plane near the core.

2.9. Corrections Using the Simulation Code

The simulation code stores the peak tune value at each scan point into a separate array. The user is allowed to make changes to the currents in the quadruploes,

sextupoles and octupoles. Changing the magnetic field in focussing quadrupoles will offset the tunes vs revolution frequency in the x-plane while changing the field in the defocussing quadrupoles will offset the tunes vs revolution frequency in the y-plane. Changing the field in sextupoles will change the slope of the tunes vs revolution frequency and changing the field in octupoles will change the curvature of the tunes vs revolution frequency. Once the user makes the desired changes the program calculates corrections, for each scan point, using Equations 2.8 with the appropriate coefficients.listed in Table 2.3.

(2.8)

$$
\begin{aligned}
\Delta v_x \;=\; & \Delta I_{QF} + (C_{x_{OCT12\_0}} + C_{x_{OCT12\_1}}(f_{rev} - f_0) + C_{x_{OCT12\_2}}(f_{rev} - f_0)^2)\Delta I_{OCT12} \\
& + (C_{x_{OCT10\_0}} + C_{x_{OCT10\_1}}(f_{rev} - f_0) + C_{x_{OCT10\_2}}(f_{rev} - f_0)^2)\Delta I_{OCT10} \\
& + (C_{x_{SEX12\_0}} + C_{x_{SEX12\_1}}(f_{rev} - f_0))\Delta I_{SEX12} \\
& + (C_{x_{SEX10\_0}} + C_{x_{SEX10\_1}}(f_{rev} - f_0) + C_{x_{SEX10\_2}}(f_{rev} - f_0)^2)\Delta I_{SEX10}
\end{aligned}
$$

$$\Delta v_y = \Delta I_{QD} + (C_{yOCT12\_0} + C_{yOCT12\_1}(f_{rev} - f_0) + C_{yOCT12\_2}(f_{rev} - f_0)^2)\Delta I_{OCT12}$$

$$+(C_{yOCT10\_0} + C_{yOCT10\_1}(f_{rev} - f_0) + C_{yOCT10\_2}(f_{rev} - f_0)^2)\Delta I_{OCT10}$$

$$+(C_{ySEX12\_0} + C_{ySEX12\_1}(f_{rev} - f_0))\Delta I_{SEX12}$$

$$+(C_{ySEX10\_0} + C_{ySEX10\_1}(f_{rev} - f_0) + C_{ySEX10\_2}(f_{rev} - f_0)^2)\Delta I_{SEX10}$$

I_{SEXxx} and I_{OCTxx} refer to the power supply currents for the sextupoles and octupoles, where xx indicates the location in the Accumulator sectors.

Coefficient	Stacking Lattice Value	Shot Lattice Value
$C_{x_{OCT12\_0}}$	8.07835×10^{-2}	-6.38059×10^{-2}
$C_{x_{OCT12\_1}}$	5.98993×10^{-4}	-5.07452×10^{-6}
$C_{x_{OCT12\_2}}$	4.25182×10^{-5}	-2.84701×10^{-5}
$C_{x_{OCT10\_0}}$	-1.78816×10^{-1}	3.71805×10^{-2}
$C_{x_{OCT10\_1}}$	-8.59186×10^{-4}	2.95619×10^{-6}
$C_{x_{OCT10\_2}}$	-1.54145×10^{-4}	1.30559×10^{-5}
$C_{x_{SEX12\_0}}$	-5.92861×10^{-3}	-3.38680×10^{-3}
$C_{x_{SEX12\_1}}$	2.15582×10^{-3}	-3.26972×10^{-3}
$C_{x_{SEX10\_0}}$	-2.22532×10^{-2}	-3.23140×10^{-3}
$C_{x_{SEX10\_1}}$	-7.42469×10^{-3}	-2.85976×10^{-3}
$C_{x_{SEX10\_2}}$	-2.06370×10^{-7}	-1.97485×10^{-11}
$C_{y_{OCT12\_0}}$	-1.10022×10^{-1}	-1.10022×10^{-1}
$C_{y_{OCT12\_1}}$	-7.06975×10^{-4}	-7.06975×10^{-4}
$C_{y_{OCT12\_2}}$	-6.19865×10^{-5}	-6.19865×10^{-5}
$C_{y_{OCT10\_0}}$	4.36403×10^{-2}	-7.81030×10^{-2}
$C_{y_{OCT10\_1}}$	3.13166×10^{-4}	-6.21317×10^{-6}
$C_{y_{OCT10\_2}}$	3.30681×10^{-5}	-2.74259×10^{-5}
$C_{y_{SEX12\_0}}$	-3.80515×10^{-2}	1.30859×10^{-3}
$C_{y_{SEX12\_1}}$	-3.59078×10^{-3}	1.26337×10^{-3}
$C_{y_{SEX10\_0}}$	3.32594×10^{-2}	1.53831×10^{-3}
$C_{y_{SEX10\_1}}$	1.72438×10^{-3}	1.36137×10^{-3}
$C_{y_{SEX10\_2}}$	-3.93965×10^{-6}	-1.21451×10^{-11}

Table 2.3. Stacking and shot lattice tune correction equation coefficients

The stacking lattice coefficients were calculated from fits to measured data. The shot lattice coefficients were derived using a tune circuits model. The coefficient calculations are outlined in Chapter 4.

2.9.1. Example of Predicted Corrections

Figure 2.3 shows the corrections predicted by the simulation code with a 10 A change in the octupole windings on the multipole magnets in the Ax10 locations, where x indicates Accumulator sectors 1 through 6, and a -10 A change in the octupole windings on the multipole magnets in the Ax12 locations. The Accumulator was configured on the stacking lattice. The algorithms predicted that the horizontal tunes should be lower by ˜0.010 units near the core and injection frequencies and the vertical tunes should be higher by ˜0.005 units near the core and by ˜0.010 near the injection frequencies. The plots in Figure 2.4 shows the tunes across the aperture before the correction and after the correction. The measured and predicted corrections match well.

Using the RF method a user could measure the tunes back and forth across the aperture as many times as they wished while making corrections after each measurement. This method provides the Antiproton Source Group with a powerful diagnostic tool.
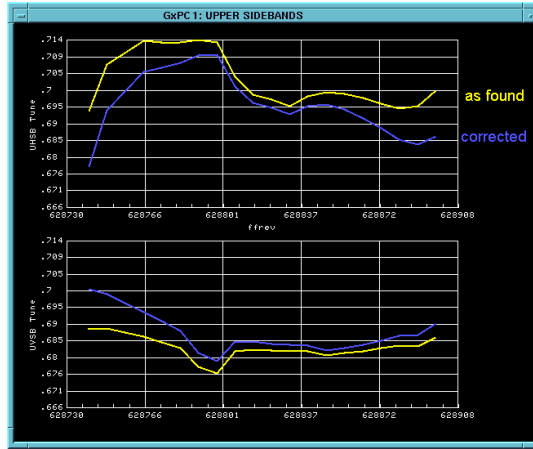
Figure 2.3. Tune measurements and correction predictions. The yellow trace shows the measured peak tune values for each scan point. The blue curve shows the change to the tunes predicted by the correction algorithms.
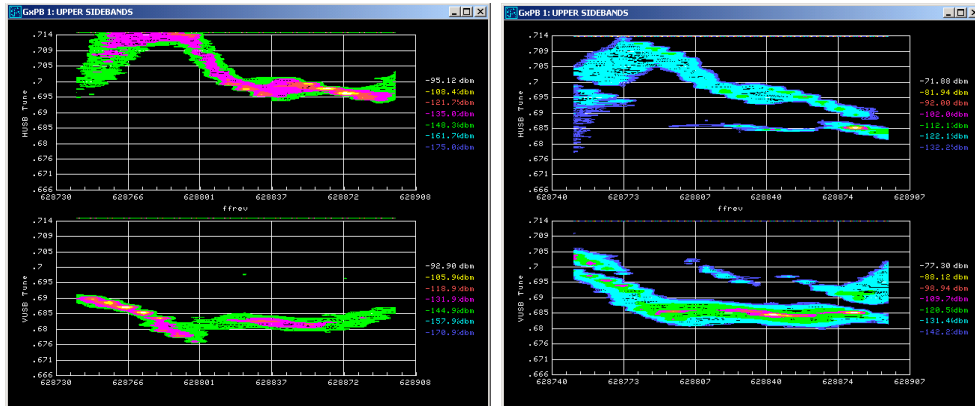
Figure 2.4. The plot on the left is the measured tunes before the corrections were applied. The plot on the right is the tunes after the corrections were applied. The algorithms predicted that the horizontal tunes should be lower by ~0.005 units near the core and injection frequencies. The algorithms predicted that the vertical tunes should be higher by ~0.010 units near the core and by ~0.010 near the injection frequencies. The measurements agree with the predictions.

CHAPTER 3

Tunes and Emmitances Measuring Sideband Power

A method similar to one developed at CERN by S. van der Meer[6] and applied
to the Accumulator by Rui Alves-Pires[7] in 1993 is presented here as a proof of
principle.

3.1. Power Measurement Method

Schottky described the statistical current fluctuations caused by a finite number
of charge carriers in 1918[6]. He showed that the noise, termed Scottky noise,
produced by each charge carrier is independent of the other charge carriers. Schottky
noise is incoherent. For particles in a storage ring, such as the Accumulator,
Schottky noise is a collection of signal pulses in the time domain, which corresponds
to a spectrum of lines in the frequency domain. The lines occur at harmonics of
the revolution frequency since the particles, circulating in the accelerator, pass
repeatedly through the Schottky detector. The combined response from all the
particles in the ring is smeared over a finite frequency range at each harmonic.
This frequency range is related to the momentum spread of the beam by Equation

3.1,

(3.1)
$$\frac{df}{f} = \frac{dp}{p}\eta$$

where η (the slip factor) is fixed by the Accumulator lattice. Each particle contributes power to each sideband independently as they circulate around the ring. The upper and lower sideband frequencies of the particles can be calculated from the revolution frequency as shown in Equations 3.2.

(3.2)
$$f_+ = (n+q)f_{rev} \text{ and } f_- = (n-q)f_{rev}$$

where n is the harmonic number, q is the fractional tune, f_{rev}, f_+ and f_- are the revolution, upper, and lower sideband frequencies of the particles, respectively.

Conversely the revolution frequency and tune of the particles can be calculated from the sideband frequencies using Equations 3.3 and 3.4 respectively:

(3.3)
$$f_{rev} = \frac{f_+ + f_-}{2n},$$

$$(3.4) \qquad q = n\frac{f_+ - f_-}{f_+ + f_-}$$

The emittance (ε) is proportional to the spectral densities ($\Psi_\pm$) of the upper and lower sidebands and can be calculated using Equation 3.5,

$$(3.5) \qquad \varepsilon = C\frac{n}{\left(\frac{dN}{df_{rev}}\right)}\frac{\Psi_+\Psi_-}{\Psi_+ + \Psi_-}$$

where

$$\Psi_\pm \propto \varepsilon\frac{dN}{df_\pm} = \frac{\varepsilon}{n \pm (q + \frac{\xi Q}{\eta})}\left(\frac{dN}{df_{rev}}\right),$$

$$\xi = \frac{p}{Q}\frac{dq}{dp} \text{ and } \eta = \frac{1}{\gamma^2} - \frac{1}{\gamma_T^2} = \frac{p}{f_{rev}}\frac{df_{rev}}{dp}$$

and Q is the full tune, ξ is the chromaticity, p is the momentum, $\frac{dq}{dp}$ is the change in tune with respect to the change in momentum, γ is the energy, γ_T is the transitional energy and $\frac{df_{rev}}{dp}$ is the change in revolution frequency with respect to the change in momentum. $\frac{dN}{df_{rev}}$ is taken from the longitudinal spectrum.
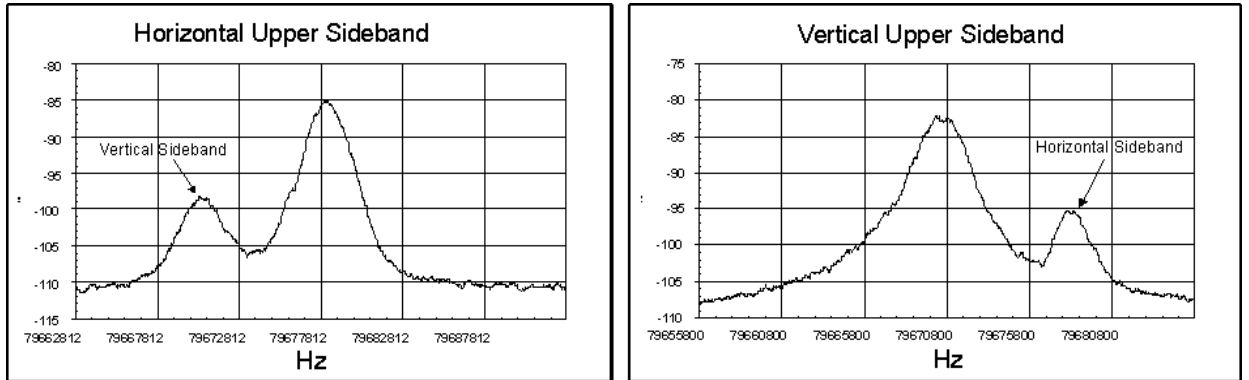
Figure 3.1. Coupling at the core revolution frequency. The plot on the left shows the vertical sideband as seen on the horizontal Schottky detector display. The plot on the left shows the horizontal sideband as seen on the vertical Schottky detector display.

3.2. Coupled Tunes at the Core Revolution Frequency

In the current running mode, the fractional Accumulator tunes at the core revolution frequency are $q_x = 0.6969$ and $q_y = 0.6845$. The tunes are close enough to be termed coupled. The plots in Figure 3.1 show the coupling in the upper sidebands. The vertical sideband is visible on a display of the horizontal schottky detector as shown in the plot on the left. Conversely, the horizontal sideband is visible on a display of the vertical schottky detector as shown in the plot on the right. Coupling the tunes leads to more efficient transvere cooling and a higher beam quality for collisions in the Tevatron but renders the S. van der Meer method of measuring tunes and emittances impractical. Therefore this technique is only used during special study periods where the core tunes are decoupled.
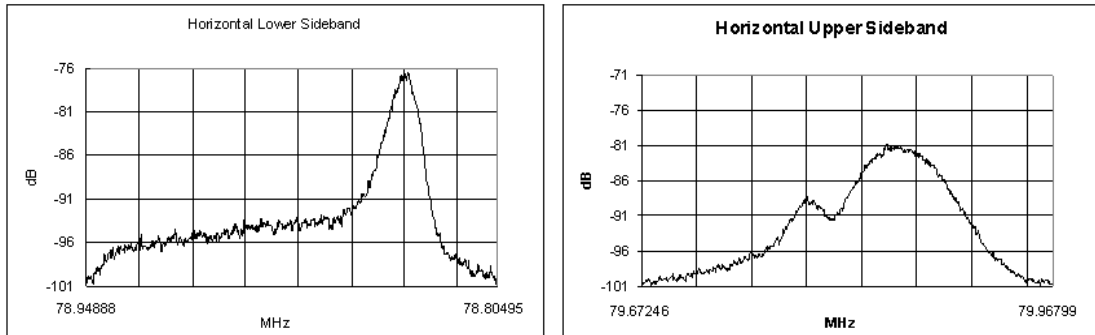
Figure 3.2. Uncoupled horizontal sidebands. The plot on the left is the lower sideband. The plot on the right is the upper sideband.
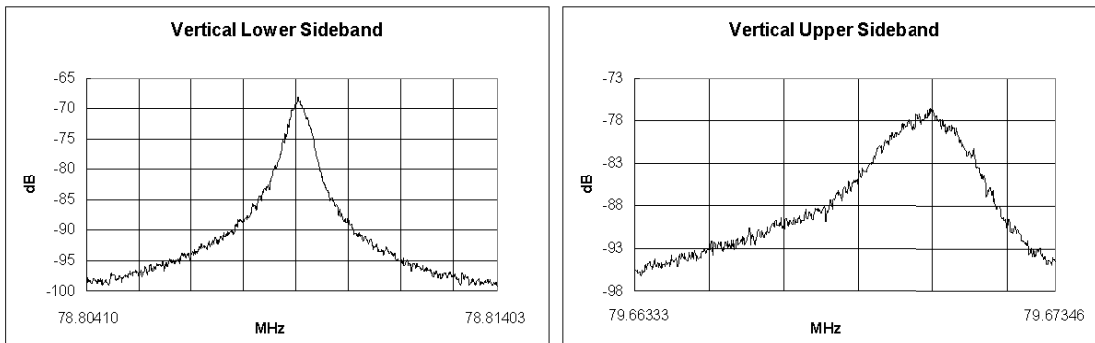
Figure 3.3. Uncoupled vertical sidebands. The plot on the left is the lower sideband. The plot on the right is the upper sideband.

3.3. Proof of Principle

To demonstrate the power measurement method on 04/23/04 the tunes at the core revolution frequency were decoupled by changing power supply settings in the Accumulator skew quadrupoles. The Accumulator was in stacking mode. Antiprotons were under the stacktail cooling pickups and there was 50 mA circulation on the core revolution frequency. The plots in Figures 3.2 and 3.3 are spectrum

51

analyzer traces of transverse Schottky detector signals showing the uncoupled sidebands.

An ACNET program was written in C to analyze the trace data. The program scans the upper sideband, in each transverse plane, and integrates the power, from the starting frequency of the sideband, to pre-determined frequency points throughout the sideband. For each of these points the program searches through the lower sideband for the frequency point with the same amount of integrated power. Revolution frequencies, tunes and emittances for these power points are calculated using Equations 3.3 , 3.4 and 3.5 , respectively, with the corresponding upper and lower sideband frequencies. Figure 3.4 shows the calculated tunes through the revolution frequencies covered by the stacktail cooling system. Figure 3.5 shows the calculated emittances through the revolution frequencies covered by the stacktail cooling system. In Equation 3.5 C is the calibration constant. The measurement at the core revolution frequency is calibrated to the emittance size measured by the dedicated system. For a $50m$ A stack $\varepsilon_x = 0.779\pi mmmr$ and $\varepsilon_y = 0.430\pi mmmr$. Therfore $C = 1.194 \times 10^{-2}$ for the horizontal measurement and $C = 7.174 \times 10^{-3}$ for the vertical measurement.
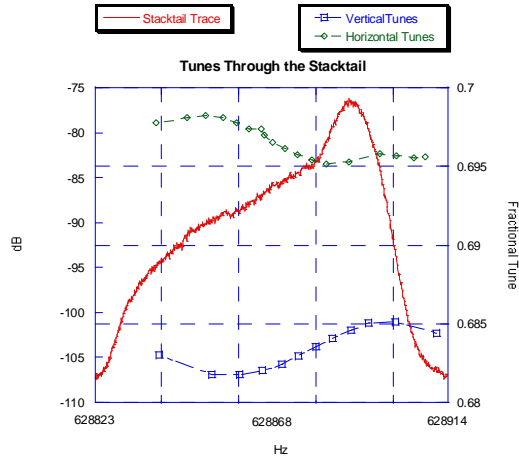
Figure 3.4. The red trace is the longitudinal Schottky stack signal. The stacktail extends from the core region to ˜628830Hz, near the central orbit. The green trace is the calculated horizontal tunes. The blue trace is the calculated vertical tunes.
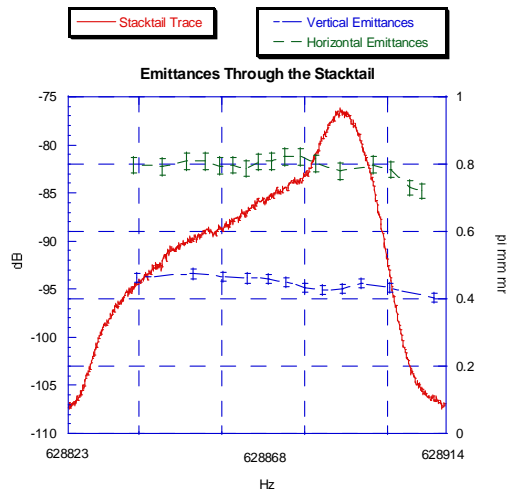

Figure 3.5. The red trace is the longitudinal Schottky stack signal. The green trace is the calculated horizintal emittances. The blue trace is the calculated vertical emittances.

Emittances and tunes can be calculated during stacking operations proving to be an advantge over the RF method in some situations. For example, if the stack rate is zero or lower than expected, while stacking in the Accumulator, the tunes could be decoupled and the power measurement method could be used to locate any resonances in the tunes under the stacktail cooling system indicating a possible problem with a magnet. Another use could be to decouple the tunes for a complete stacking cycle and using the power measurement method at several stack sizes to characterize tunes and emittances with respect to the number of antiprotons in the stack. However, since the stacktail cooling system only covers approximately half of the momentum aperture, the power measurement method cannot measure the tunes near the injection revolution frequencies.

CHAPTER 4

Tune Correction Coefficients and the Lattice Model

The sextupoles and octupoles located in the Ax10 and Ax12 locations, where x indicates Accumulator sectors 1 through 6, (Figure 1.2) are wound on a common frame. These magnets are termed multipoles. The sextupole and octupole fields are formed by the shape and location of separate windings, rather than the number of poles, and are powered by separate supplies. Since the multipoles are located in the high dispersion straight sections different momentum particles will experience different field strengths and exhibit different tunes. The sextupole and octupole fields in the multipoles are termed tune circuits.

The correction equation coefficients for the stacking (Section 4.1) and shot (Section 4.2) lattices were derived using two separate methods[8].

4.1. Stacking Lattice Coefficients

The stacking lattice coefficients were derived by applying a fit to measured data. The measurements of the tune circuits were made in the months between December 2001 and April 2002. For each tune circuit the tunes at predetermined revolution frequencies were measured at several power supply settings. From the
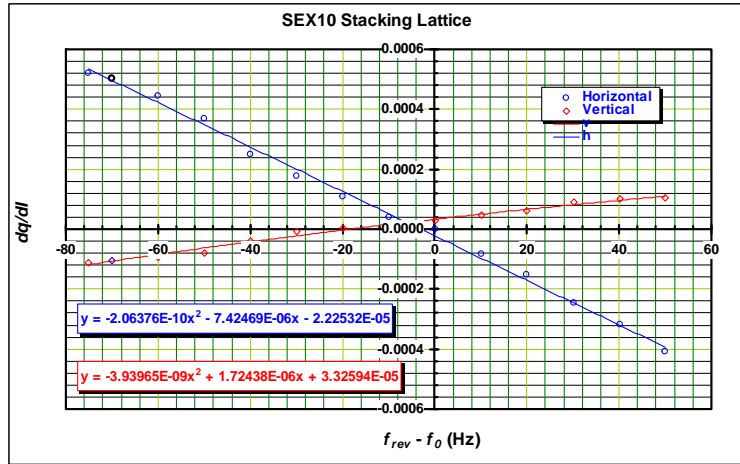
Figure 4.1. Fits to $\frac{dq}{dI}$ curves for the sextupoles in the Ax10 locations on the stacking lattice.
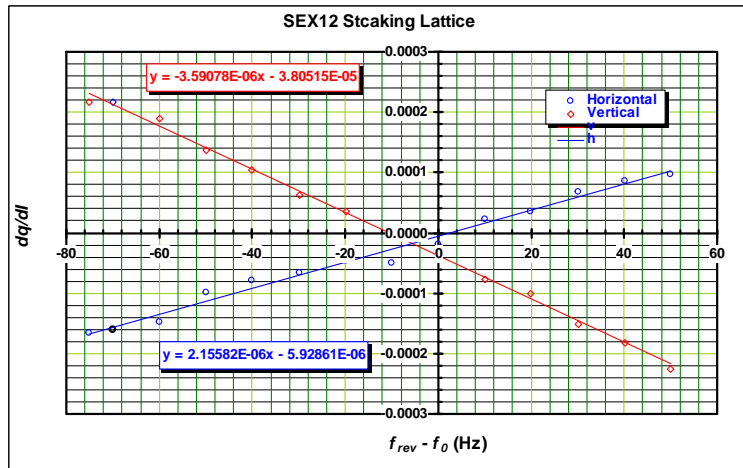

Figure 4.2. Fits to $\frac{dq}{dI}$ curves for the sextupoles in the Ax12 locations on the stacking lattice.

resulting data tune changes with respect to current changes ($\frac{dq}{dI}$) were calculated.

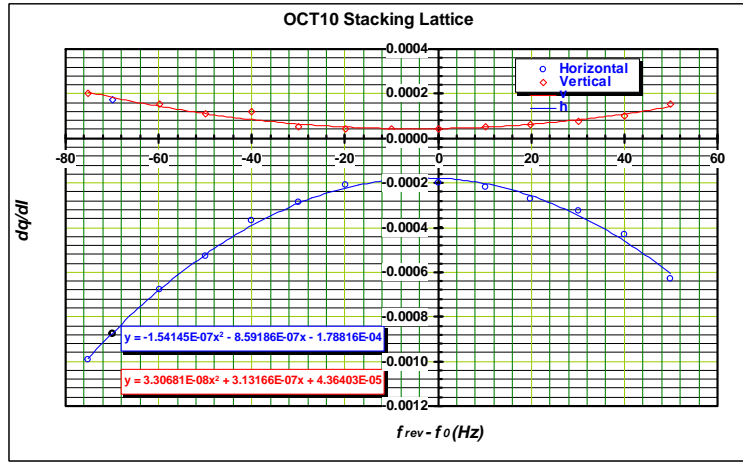Fits were applied to the $\frac{dq}{dI}$ curves. Figures 4.1 and 4.2 shows the fits, including the

Figure 4.3. Fits to $\frac{dq}{dI}$ curves for the octupoles in the Ax10 locations on the stacking lattice.
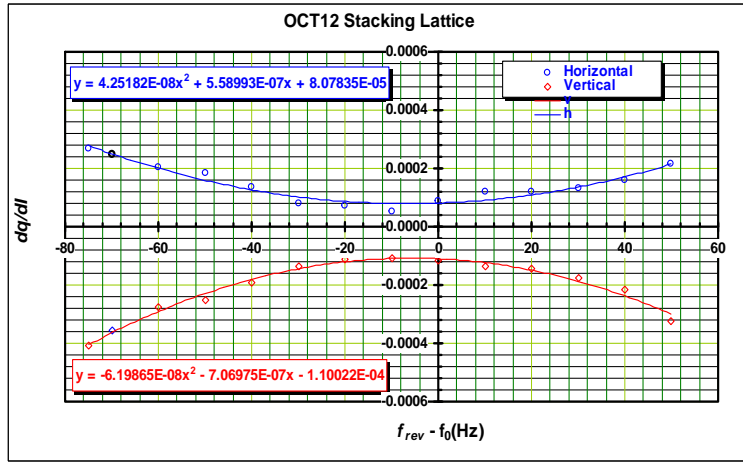
Figure 4.4. Fits to $\frac{dq}{dI}$ curves for the octupoles in the Ax12 locations on the stacking lattice.

correction equation coefficients, for the sextupoles. Figures 4.3 and 4.4 shows the fits, including the correction equation coefficients, for the octupoles.

4.2. Shot Lattice Coefficients

The development and operation of the shot lattice was established in the months of May and June of 2002. Unlike on the stacking lattice no study time was given to measure the tune circuits on the shot lattice. Another method was needed to derive the tune correction equation coefficients for the shot lattice. The solution was to take the following steps:

- Develop a tune circuits model using MathCad.
- Compare the model to the the measured stacking lattice $\frac{dq}{dI}$ curves using the stacking lattice functions.
- Enter the shot lattice functions into the model to create shot lattice $\frac{dq}{dI}$ curves.
- Apply fits to the shot lattice $\frac{dq}{dI}$ curves to produce the shot lattice tune correction equation coefficients.

To develop the model and the correction algorithms (Subsection 4.2.7) many parameters were defined and calculated as outlined through Subsection 4.2.6.

4.2.1. Define Constants, Units and Accelerator Parameters

Electron Charge	$e_c = 1.60217733 \times 10^{-19}\,\mathrm{C}$
Speed of Light	$c = 299792458\,\frac{\mathrm{m}}{\mathrm{s}}$
Electron Volt	$\mathrm{eV} = e_c\,\mathrm{V},\ \mathrm{MeV} = 10^6\,\mathrm{eV}$
Antiproton Mass	$m_p = 938.27231\,\frac{\mathrm{MeV}}{\mathrm{c}^2}$
Number of Accumulator Lattice Sections	$N_{Sec} = 6$
δ	$\frac{-1}{\eta}\frac{\Delta f_{rev}}{f_{rev}}$
Central Orbit Momentum	$p_0 = 8803.89\,\frac{\mathrm{MeV}}{\mathrm{c}}$
Central Orbit Circumference	$L_0 = 474.0535\,\mathrm{m}$
Central Orbit Revolution Frequency	$f_0 = 628840\,\mathrm{Hz}$
Core Revolution Frequency	$f_c = 628888\,\mathrm{Hz}$
Extraction Orbit Revolution Frequency	$f_e = 628765\,\mathrm{Hz}$
Dipole Field	$B_0 = 16815.752\,\mathrm{G}$
Central Orbit Radius of Curvature in Main Dipoles	$\rho = \frac{p_0}{B_0 e_c} = 17.463754\,\mathrm{m}$

4.2.2. η on the Stacking Lattice

The quantity η is constant across the momentum aperture on the shot lattice, however, it is not constant across the momentum aperture on the stacking lattice.
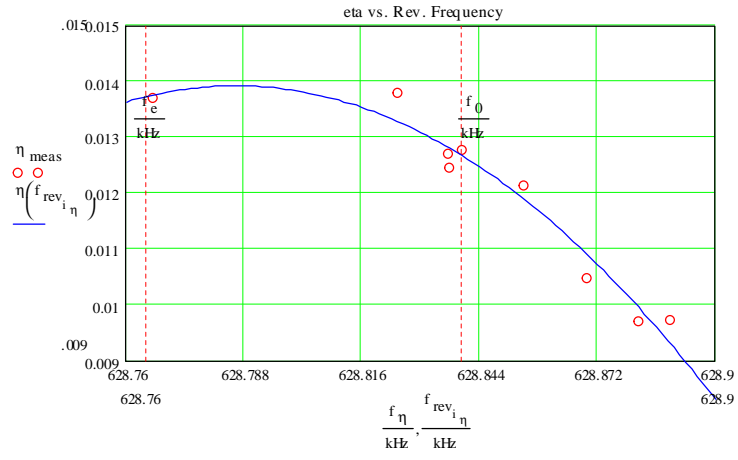
Figure 4.5. Calculated fit to the measured η at various revolution frequencies on the stacking lattice.

η varies as a function of f_{rev} and has been measured. The measured η versus f_{rev} was fit to the polynomial in Equation 4.1. Plot 4.5 shows the fit.

(4.1) $\eta(f) = -4.327 \times 10^{-7}(f_{rev} - f_0)^2 - 4.670 \times 10^{-5}(f_{rev} - f_0) + 1.266 \times 10^{-2}$

4.2.3. Kinematical Quantities

Equations 4.2 show calculations of η_0, β_0, γ_0 and γ_{t0} on the central orbit of the Accumulator.

(4.2) $$\eta_0 = \eta(f_0) = 0.0024 \qquad \beta_0 = \frac{L_0 f_0}{c} = 0.994,$$

$$\gamma_0 = (1 - \beta_0^2)^{\frac{-1}{2}} = 9.435 \qquad \gamma_{t0} = (\eta_0 + \frac{1}{\gamma_0^2})^{\frac{-1}{2}} = 8.541$$

Equations 4.3 show calculations for E, β, p, γ, γ_t and the orbit length (L_{orb}) as a function of momentum for any orbit in the Accumulator.

(4.3) $$E_p(p) = \sqrt{(p\,c)^2 + (m_p\, \overset{2}{c})^2} \qquad \beta_p(p) = \frac{p\,c}{E_p(p)},$$

$$p(f) = p_0 e^{-\int_0^{f-f_0} \frac{1}{(f_0+x)\eta(f_0+x)}dx} \qquad E(f) = \sqrt{(p(f)\,c)^2 + (m_p\,\overset{2}{c})^2},$$

$$\gamma(f) = \frac{E(f)}{m_p c^2} \qquad \beta(f) = \frac{p(f)\,c}{E(f)},$$

$$\gamma_t(f) = (\eta(f) + \frac{1}{\gamma_t(f)^2})^{\frac{-1}{2}},$$

$$L_{orb}(f) = L_0 e^{-\int_{f_0}^{f} \frac{1}{x\eta(x)\gamma_t(x)^2} dx},$$

$$\delta p(f) = \frac{p(f) - p_0}{p_0},$$

$$p_c = p(f_c) = 8743.718 \frac{\text{MeV}}{\text{c}}$$

4.2.4. Multipole Parameters

Stength in the multipole magnets as a function of power supply current for the quadrupole, sextupole and octupole fields are shown in Equations 4.4, 4.5 and 4.6,respectively.

$$(4.4) \quad B_1(I_S, I_O) = (2.030764 \times 10^{-6} \frac{\text{T}}{\text{A}}) I_S + (2.486613 \times 10^{-4} \frac{\text{T}}{\text{A}}) I_O$$
$$+ (3.523344 \times 10^{-7} \frac{\text{T}}{\text{A}^2}) I_S I_O + (-4.4 \times 10^{-9} \frac{\text{T}}{\text{A}^3}) I_S I_O^2,$$

$$B_1(I_S, I_O, \Delta I_S, \Delta I_O) = B_1(I_S + \Delta I_S, I_O + \Delta I_O) - B_1(I_S, I_O)$$

$$(4.5) \quad B_2(I) = (1.097079 \times 10^{-6}\frac{\text{T}}{\text{m A}^2})I^2$$

$$-(1.193167 \times 10^{-2}\frac{\text{T}}{\text{m A}})I - 6.006515 \times 10^{-2}\frac{\text{T}}{\text{m}},$$

$$B_2(I, \Delta I) = B_2(I + \Delta I) - B_2(I),$$

$$(4.6) \quad B_3(\Delta I) = (3.127722 \times 10^{-1}\frac{\text{T}}{\text{m}^2\,\text{A}})\Delta I$$

4.2.5. Bus Currents

The sextupole power supply current in the Ax10 locations, where x refers to sectors 1 through 6, is nominally set to 404 A. The sextupole power supply current in the Ax12 locations is nominally set to 581 A. The octupole power supply current in the Ax10 locations is nominally set to 52.01 A and 64.04 A in the Ax12 locations. The possibility of a polarity change must be included and is defined as $Polarity_{i_M} = -1(-1)^{i_M}$.

4.2.6. Stacking Lattice Parameters at the Multipole Magnets

In the Ax10 locations β_x is $45.527\,\text{m}$, β_y is $12.568\,\text{m}$ and D_x is $7.758\,\text{m}$. In the Ax12 locations β_x is $18.486\,\text{m}$, β_y is $29.554\,\text{m}$ and D_x is $6.976\,\text{m}$.

4.2.7. Correction Algorithms

Equations 4.7 shows the developed tune circuits model.

$$(4.7) \quad \delta\nu_{x0}(\delta, \Delta I_{SEX}, \Delta I_{OCT})$$

$$= \frac{N_{Sec}e_c}{4\pi p_0}[(1-\delta)\sum_{i_M}(Polarity_{i_M}\beta_{x_{i_M}}B_1(I_{SEX_{i_M}}, I_{OCT_{i_M}}, \Delta I_{SEX_{i_M}}, \Delta I_{OCT_{i_M}}))$$

$$+\delta\sum_{i_M}(Polarity_{i_M}\beta_{x_{i_M}}D_{x_{i_M}}B_2(I_{SEX_{iM}}, \Delta I_{SEX_{i_M}}))$$

$$+\frac{1}{2}\delta^2\sum_{i_M}(Polarity_{i_M}\beta_{x_{i_M}}D^2_{x_{i_M}}B_3(\Delta I_{OCT_{i_M}})],$$

$$\delta\nu_{y0}(\delta, \Delta I_{SEX}, \Delta I_{OCT})$$

$$= \frac{N_{Sec}e_c}{4\pi p_0}[(1-\delta)\sum_{i_M}(Polarity_{i_M}\beta_{y_{i_M}}B_1(I_{SEX_{i_M}}, I_{OCT_{i_M}}, \Delta I_{SEX_{i_M}}, \Delta I_{OCT_{i_M}}))$$

$$+\delta\sum_{i_M}(Polarity_{i_M}\beta_{y_{i_M}}D_{x_{i_M}}B_2(I_{SEX_{iM}}, \Delta I_{SEX_{i_M}}))$$

$$+\frac{1}{2}\delta^2\sum_{i_M}(Polarity_{i_M}\beta_{y_{i_M}}D^2_{x_{i_M}}B_3(\Delta I_{OCT_{i_M}})]$$
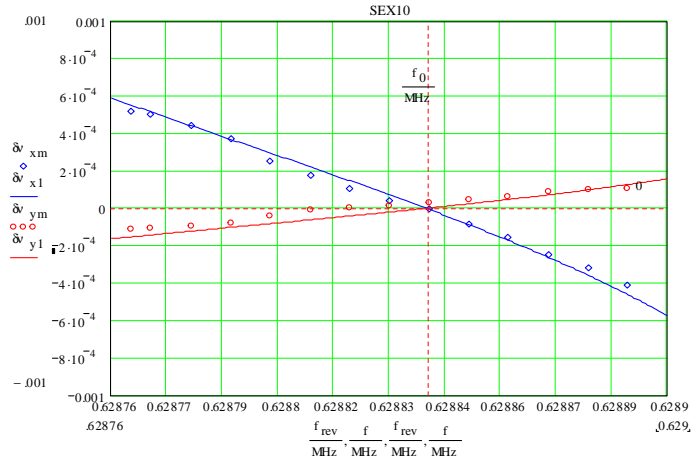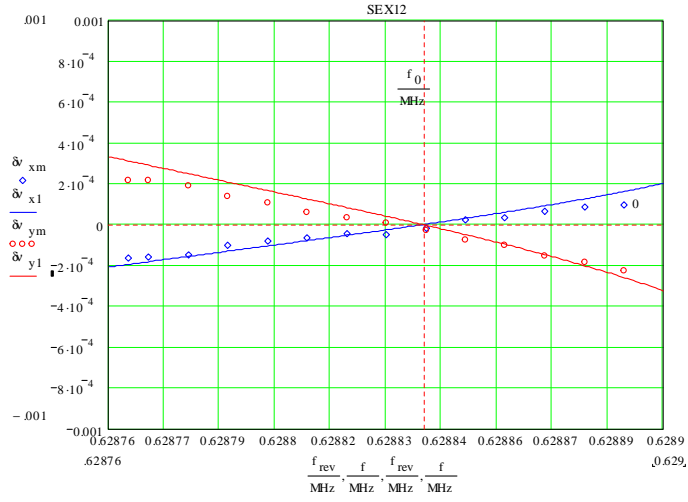
Figure 4.6. Model predictions compared to measured $\frac{dq}{dI}$ data for sextupoles in the Ax10 locations on the stacking lattice.

4.2.8. Compare Fits to Measured Values on the Stacking Lattice

The plots in Figures 4.6 and 4.7 show the measured data compared to the model prediction for a 1 A change in the Ax10 and Ax12 location sextupoles, respectively. The model predictions match the measured data well. Figures 4.8 and 4.9 show the measured data compared to the model prediction for a 1 A change in the Ax10 and Ax12 location octupoles, respectively. The model predictions match well for the Ax12 octupoles. The model diverges from the measurements by as much as 20% near the injection region for the Ax10 octupoles. This has not been a problem during operations.

Figure 4.7. Model predictions compared to measured $\frac{dq}{dI}$ data for sextupoles in the Ax12 locations on the stacking lattice.
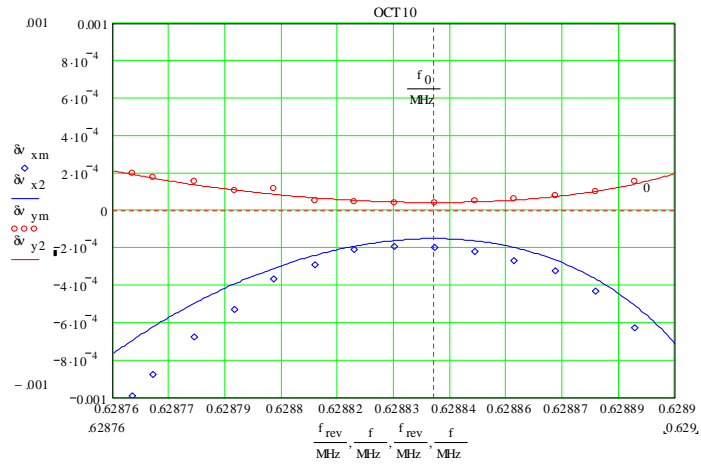

Figure 4.8. Model predictions compared to measured $\frac{dq}{dI}$ data for octupoles in the Ax10 locations on the stacking lattice.
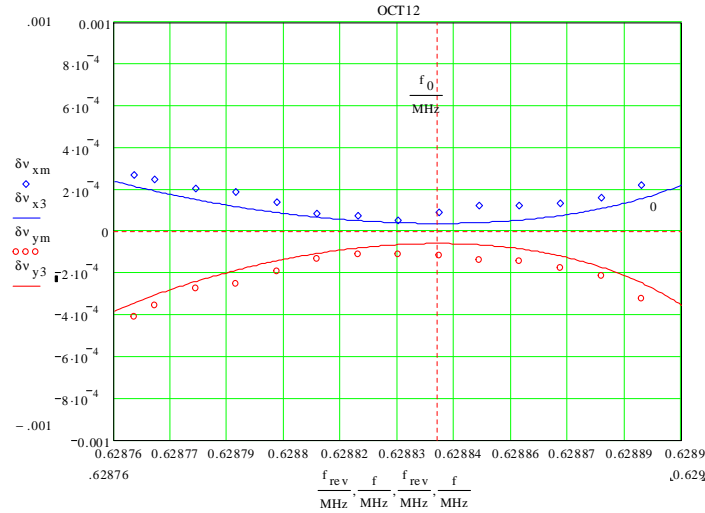
66

Figure 4.9. Model predictions compared to measured $\frac{dq}{dI}$ data for octupoles in the Ax12 locations on the stacking lattice.

4.2.9. Predicted Tune Changes on the Shot Lattice

The shot lattice functions in the Ax10 locations are $\beta_x = 23.511\,\text{m}$, $\beta_y = 11.192\,\text{m}$ and $D_x = 8.519\,\text{m}$. In the Ax12 locations they are $\beta_x = 12.289\,\text{m}$, $\beta_y = 29.554\,\text{m}$ and $D_x = 7.462\,\text{m}$. Using these lattice functions in the model will give predicted tune changes on the shot lattice. Figures 4.10 and 4.11 show the model prediction for a 1 A change in the Ax10 and Ax12 location sextupoles, respectively. Figures 4.12 and 4.13 show the model prediction for a 1 A change in the Ax10 and Ax12 location octupoles, respectively.
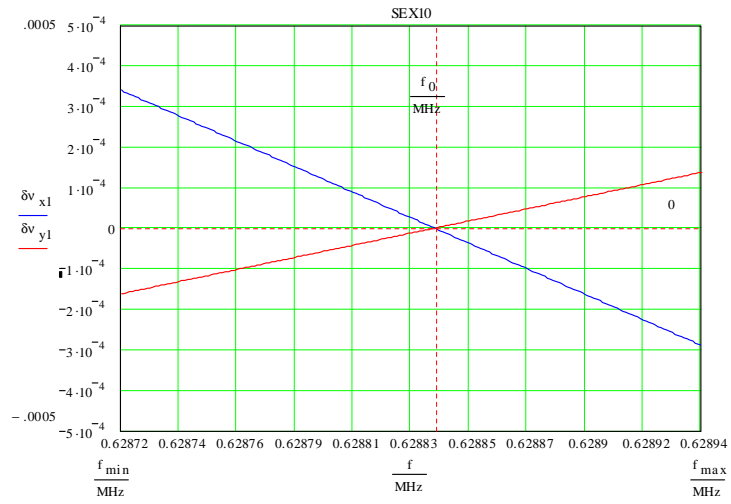
Figure 4.10. Model prediction $\frac{dq}{dI}$ curves for sextupoles in the Ax10 locations on the shot lattice.
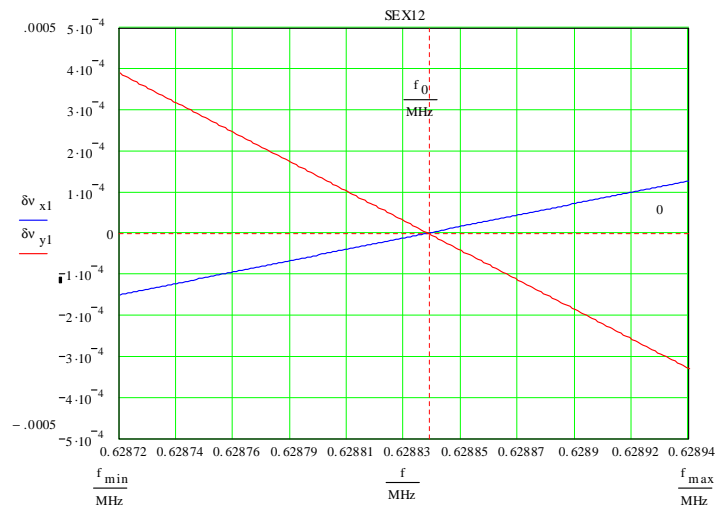

Figure 4.11. Model prediction $\frac{dq}{dI}$ curves for sextupoles in the Ax12 locations on the shot lattice.
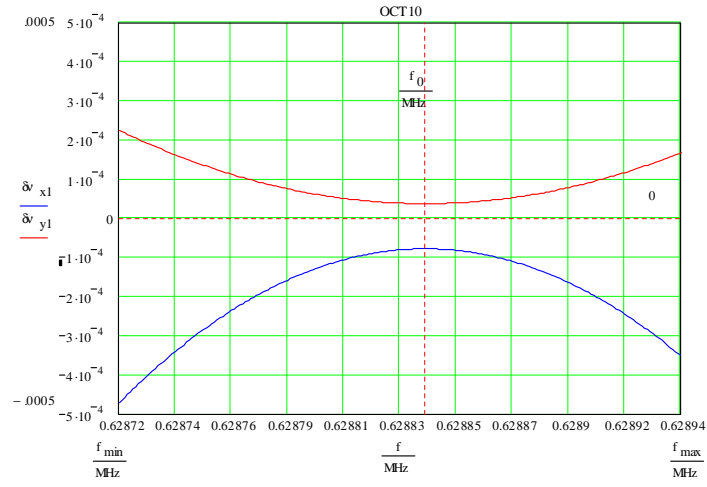
Figure 4.12. Model prediction $\frac{dq}{dI}$ curves for octupoles in the Ax10 locations on the shot lattice.
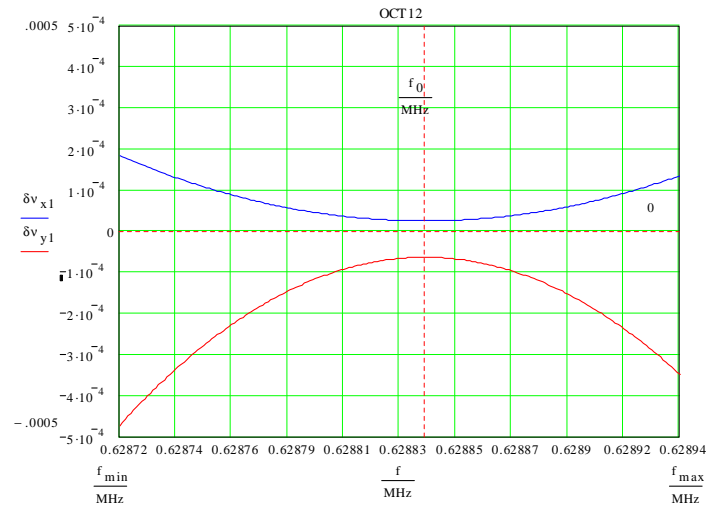

Figure 4.13. Model prediction $\frac{dq}{dI}$ curves for octupoles in the Ax12 locations on the shot lattice.
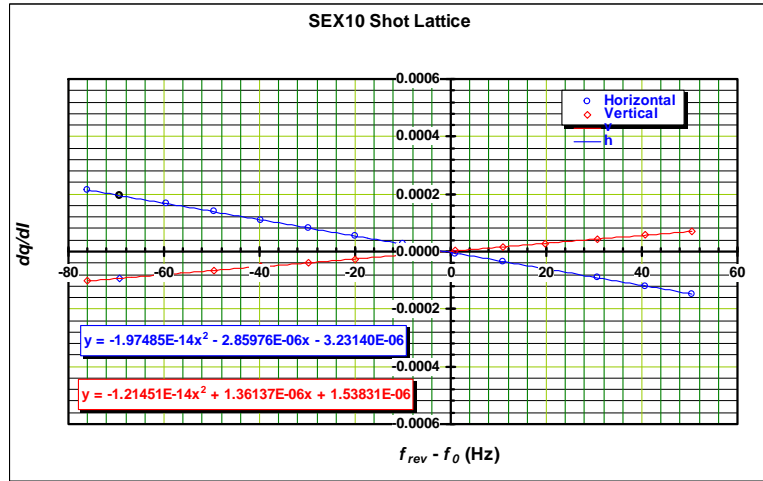
69

Figure 4.14. Fits to $\frac{dq}{dI}$ curves predicted by the model for the sextupoles in the Ax10 locations on the shot lattice.

4.2.10. Fits to the Shot Lattice $\frac{dq}{dI}$ Curves

Figures 4.14 and 4.15 show the fits, including the tune correction equation coefficients, to the shot lattice model prediction for a 1 A change in the Ax10 and Ax12 location sextupoles, respectively.

Figures 4.16 and 4.17 show the fits, including the tune correction equation coefficients, to the shot lattice model prediction for a 1 A change in the Ax10 and Ax12 location octupoles, respectively.
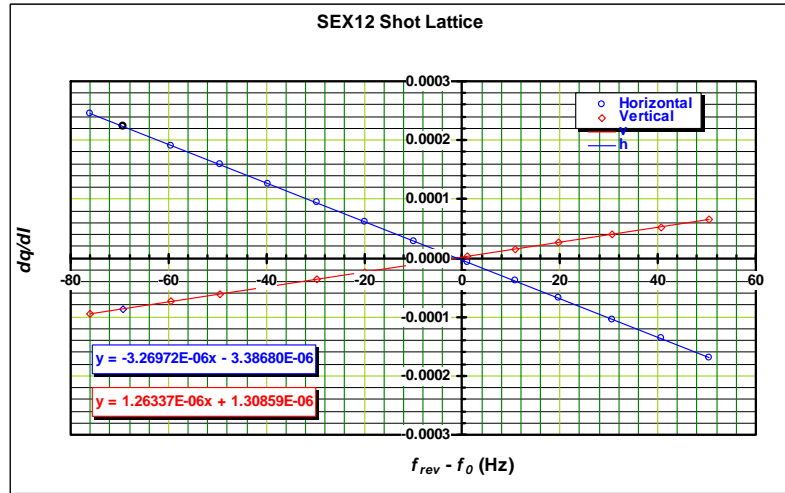
Figure 4.15. Fits to $\frac{dq}{dI}$ curves predicted by the model for the sextupoles in the Ax12 locations on the shot lattice.
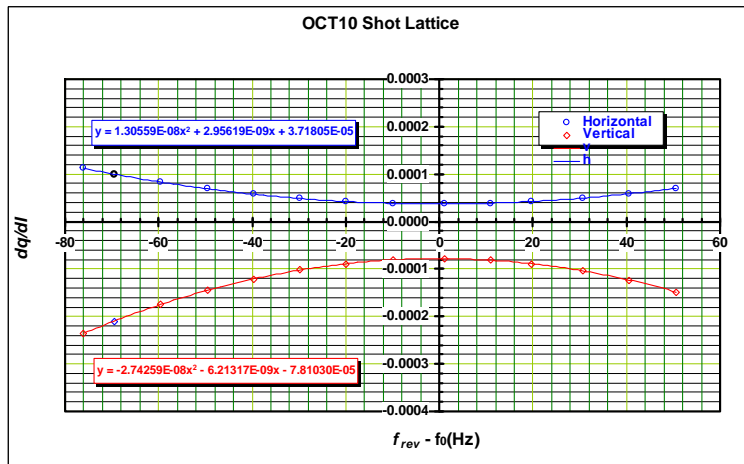

Figure 4.16. Fits to $\frac{dq}{dI}$ curves predicted by the model for the octupoles in the Ax10 locations on the shot lattice.

OCT12 Shot Lattice

$y = 1.10004E-08x^2 + 1.96009E-09x + 2.46537E-05$

Horizontal
Vertical

$y = -2.84701E-08x^2 - 5.07452E-09x - 6.38059E-05$

dq/dI
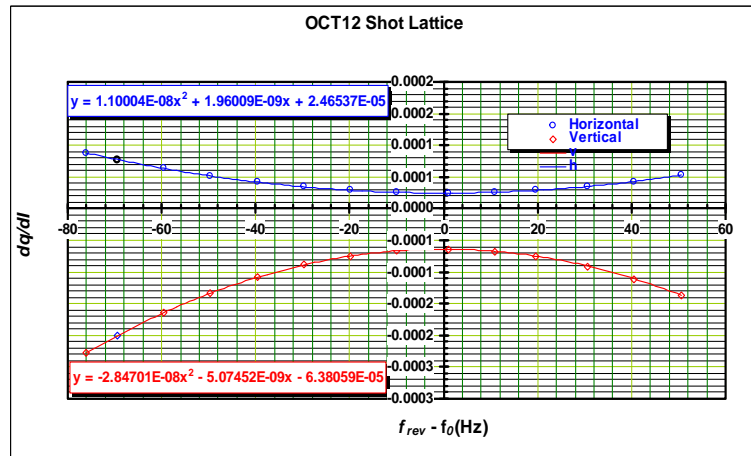
$f_{rev} - f_0\text{(Hz)}$

Figure 4.17. Fits to $\frac{dq}{dI}$ curves predicted by the model for the octupoles in the Ax12 locations on the shot lattice.

CHAPTER 5

Summary and Conclusions

It is important to know the tunes and emittances across the momentum aperture of an accelerator, especially a storage ring such as the Accumulator. Methods and tools must be developed to correct for any anomalies and to keep the machine operating within a stable space.

To measure the tunes across the aperture during Tevatron Run I beam would be bunched and moved with RF, by hand, to various revolution frequencies. Tunes would be calculated one at a time from Schottky detector spectrum analyzer traces. The tunes were manually entered into a separate simulation code to predict and apply any corrections. The measurements would then be taken again. The method was similar in nature to the RF method described in Chapter 2, however, it would take two knowledgable people four to eight hours to setup and execute. During special circumstances the Accumulator would run with no coupling at the core revolution frequency. The method first developed by S. van der Meer and adapted by Rui Alves-Pires in 1993, for the Accumulator at Fermilab, was used in the instances. During the current collider run the Accumulator runs with coupling at

the core frequency so this power measurement method, as described in Chapter 3.1 becomes difficult.

In the beginning of Tevatron Run II, as in Run I, beam was bunched and moved with RF by hand, although a VSA was now available. This was an improvement, especially in the display of the data, yet there were still limitations. Two experienced people were needed, only two sidebands could be recorded during a measurement, data would have to be stored in a file on the VSA or transfered to a floppy disk for later analysis and tune values were calculated, by hand, and manually entered into a separate simulation. The RF method described in Chapter 2 is a vast improvement. Once a person is familiar with the software a two sideband measurement would take one person 10 to 15 minutes to execute. A four sideband measurement would take 20 to 30 minutes. Peak values are automatically loaded into the simulation code so a second measurement could be done within minutes. Data can be stored in a file on the controls system which could be analyzed by anyone with a console.

Using the program written to move the beam using ARF-3 is now the primary method for measuring the tunes across the aperture and will be used for maintaining the tunes as well as measuring and adjusting tunes for any Accumulator lattice changes. One such change will happen in the near future. The Recycler ring is currently being commissioned. When it is integrated into daily operations the

Accumulator will no longer transfer antiprotons to the Tevatron for collider stores. The Accumulator will transfer antiprotons to the Recycler where larger stacks can be accumulated. There is a ~40 MeV energy difference between the Accumulator and the Recycler. Since the Recycler uses permanent magnets the energy in the Recycler is fixed. 8 GeV energies in all of the other machines will need to be adjusted to match the Recycler energy. This adjustment will require a change to the Accumulator lattice. Measuring and adjusting the tunes across the aperture will be essential during this change. The RF method will be the method used.

Although the power measurement method is not the primary tool used to measure the tunes across the aperture it does have two advantages over the RF method. Emittances are calculated and tunes are measured during stacking operations. This could prove to be useful. For example, if the stack rate is zero or lower than expected while stacking in the Accumulator the tunes could be decoupled and the power measurement method could be used to locate any possible resonances in the tunes across the aperture indicating a possible problem with a magnet. Another use could be to decouple the tunes for a complete stacking cycle and using the power measurement method at several stack sizes to characterize tunes and emittances with respect to the number of antiprotons in the stack.

These two methods of measuring the tunes across the aperture compliment each other and give the Antiproton Source Group great versatility.

References

[1] Elvin Harms and Jim Morgan, *The Antiproton Source Rookie Book,* Fermi National Accelerator Laboratory, August 1999.

[2] A. V. Tollestrup and G. Dugan, *Physics of High Energy Particle Accelerators,* AIP Conf. Proc. 105, New York, 1983.

[3] *Hewlitt Packard 89440A DC to 1.8 GHz Data Sheet.*

[4] S. Y. Lee, *Accelerator Physics,* (World Scientific Publishing, Singapore, 1999).

[5] D. A. Edwards and M. J. Syphers, *An Introduction to the Physics of High Energy Accelerators,* (John Wiley and Sons, Inc, N. Y., 1993).

[6] S. van der Meer *DIAGNOSTICS WITH SCHOTTKY NOISE,* Lecture given at the Joint US-CERN School on Beam Observation, Diagnosis and Correction, October 1988, Capri, Italy.

[7] Rui Alves-Pires *Measurement of Transverse Emittances as a Function of Revolution Frequency and Beam Current in the Accumulator,* Pbar Note #548, Fermi National Accelerator Laboratory, August 1993.

[8] S. Werkema, private communications.

[9] Fermilab Personnel, *DESIGN REPORT TEVATRON 1 PROJECT,* Fermi National Accelerator Laboratory, September 1984.